Helsinki University of Technology Radio Laboratory Publications
Teknillisen korkeakoulun Radiolaboratorion julkaisuja
Espoo, September 2007 REPORT S 290

MINIATURIZATION AND EVALUATION METHODS OF MOBILE TERMINAL ANTENNA STRUCTURES

Juha Villanen

Dissertation for the degree of Doctor of Science in Technology to be presented with due permission for public examination and debate in Auditorium S4 at Helsinki University of Technology (Espoo, Finland) on the 2nd November 2007 at 12 o'clock noon.

Helsinki University of Technology
Department of Electrical and Communications Engineering
Radio Laboratory

Teknillinen korkeakoulu
Sähkö- ja tietoliikennetekniikan osasto
Radiolaboratorio

Distribution:

Helsinki University of Technology

Radio Laboratory

P.O. Box 3000

FI-02015 TKK

Tel. +358-9-451 2252

Fax. +358-9-451 2152

ISBN 978-951-22- 8963-9 (printed)
ISBN 978-951-22- 8964-6 (electronic)
http://lib.tkk.fi/Diss/2007/isbn9789512289646

ISSN 1456-3835

Otamedia Oy

Espoo 2007

Preface

The work for this thesis has been done at the Radio Laboratory of Helsinki University of Technology during 2003-2007. The work has been funded partly by the Graduate School of Electrical and Communications Engineering. My postgraduate studies have been additionally supported by Emil Aaltonen Foundation, HPY Foundation, Nokia Foundation, and Elektroniikkainsinöörien Seura (EIS). Part of the work has been done in projects funded by Nokia Research Center. The support of all the mentioned parties is gratefully acknowledged.

I would like to express my deep gratitude to my supervisor Prof. Pertti Vainikainen for the opportunity to work in very interesting research projects as part of a recognized antenna group. Thank you for the excellent guidance, and those numerous teaching discussions and ideas that have made the work possible.

I warmly thank Dr. Clemens Icheln for instructing my thesis work. Particularly, I want to thank you for the many good ideas, suggestions, and discussions that have been essential for this thesis. I would also like to thank you for reviewing my thesis.

One of the best experts in the field of mobile terminal antennas, Dr. Jani Ollikainen, deserves special thanks for sharing his wisdom and valuable ideas. The principle “simulate and measure the same thing” I have at least tried to follow during my thesis. I would also like to thank you for providing the possibility to work in very interesting projects.

All my colleagues at the Radio Laboratory deserve thanks for their assistance and for making the laboratory a pleasant place to work. I would especially like to thank Pasi Suvikunnas, Kati Sulonen, Jari Salo, Jari Holopainen, Milla Mikkola, and Juho Poutanen for their help and cooperation. Lauri Laakso deserves acknowledgement for helping me with mechanical realization of prototypes. I would also like to thank Dr. An-Ping Zhao and Professor Athanasios Kanatas for reviewing the thesis and for their comments and suggestions.

I am most grateful to my parents for their endless support and encouragement during the whole course of my studies. Finally, I would like to express my dearest thanks to my loving and caring wife Sanna for her support and patience during the work, and to my dear daughter Alisa for making me laugh every day.

Abstract

In recent years, the trend in the mobile communications market has been towards thinner and mechanically more complex terminal devices, which are able to operate in several wireless systems. Due to this development, miniaturization and performance enhancement of internal mobile terminal antennas have become major challenges for the industry of the field. Not only should an internal antenna be small in size and broadband, it must also be able to ensure reliable power transmission in a real multipath propagation environment. A well-known way to improve the reliability of a radio connection is to use multi-antenna reception in the mobile terminal. In multiple-input multiple-output (MIMO) systems, multiple antennas are additionally used at the base station. In both cases, fast and reliable methods are needed for the performance evaluation of multi-antenna terminals.

In the first part of this thesis, the main benefits, drawbacks and applications of coupling element based mobile terminal antenna structures are studied, with special emphasis on antenna miniaturization. Optimum shaping and placement of capacitive coupling elements are first studied in this work. Next, it is demonstrated by simulations and measurements that the bandwidth-to-volume ratio of a mobile terminal antenna structure can be improved significantly by using optimized coupling elements instead of traditional self-resonant antenna elements. To facilitate the implementation of coupling element based multi-resonant antenna structures, a theoretical study on the dual-resonant impedance matching of non-resonant coupling elements is also presented. The feasibility of coupling elements for multi-band terminals is demonstrated with a novel quad-band GSM antenna, which consumes a total volume of only 0.7 cm^3. Finally, a novel frequency tunable matching circuitry designed for non-resonant coupling elements is introduced.

In this work, also the bandwidth, efficiency in talk position, and SAR (specific absorption rate) of mobile phone antennas are studied as a function of frequency over wide frequency band (0.6 GHz - 6 GHz) by applying the idea of coupling elements. The results show that below 3 GHz the three parameters are strongly affected by the resonant wavemodes of the chassis, whereas above 3 GHz, the wavemodes of the coupling element dominate. In addition to the above, the resonant wavemodes of the chassis of a clamshell phone are investigated in this work by using coupling elements. The results bring out several challenges, such as a non-radiating resonance, that an antenna designer may face with clamshell phones.

The second part of this thesis concentrates on the performance evaluation of mobile terminal multi-antenna configurations. First, the accuracy of a novel measurement based antenna test bed (MEBAT) is thoroughly studied. After this, the performance of several mobile terminal multi-antenna configurations is systematically investigated using the MEBAT. The emphasis is kept on the power reception properties (effective array gain or *EAG*) of the multi-antenna configurations. An accurate and fast theoretical way of predicting the median *EAG* of an antenna configuration is proposed in the work. Based on a comprehensive analysis of the theoretical and empirical *EAG* results, guidelines for optimum radiation pattern characteristics of a multi-antenna configuration are given. Based on the eigenvalue dispersion and capacity results obtained in the studied MIMO environments, it is concluded that it may be difficult to affect the spatial multiplexing properties of a MIMO system by means of handset antenna design. The presented results indicate that a handset antenna designer should mainly focus on maximizing the *EAG*.

Tiivistelmä

Viime vuosina yleinen kehityssuunta matkaviestinmarkkinoilla on ollut kohti ohuempia ja mekaanisesti monimutkaisempia päätelaitteita, jotka kykenevät toimimaan useissa langattomissa järjestelmissä. Tämän kehityksen johdosta matkapuhelinten sisäisten antennien koon pienentäminen ja suorituskyvyn parantaminen ovat muodostuneet merkittäviksi haasteiksi alan teollisuudelle. Sen lisäksi, että sisäisen antennin tulee olla pienikokoinen ja laajakaistainen, tulee sen myös kyetä takaamaan luotettava tehonsiirto todellisessa monitie-etenemisympäristössä. Hyvin tunnettu tapa radioyhteyden luotettavuuden parantamiseksi on hyödyntää moniantennivastaanottoa matkapuhelimessa. Multiple-input multiple-output (MIMO)-järjestelmissä useita antenneja hyödynnetään lisäksi tukiasemassa. Kummassakin tapauksessa tarvitaan nopeita ja luotettavia menetelmiä matkapuhelinten moniantennirakenteiden suorituskyvyn arvioimiseksi.

Työn ensimmäisessä osassa tutkitaan kytkentäelementteihin perustuvien antennirakenteiden tärkeimpiä hyötyjä, haittoja ja sovelluksia painottaen antennien koon pienentämistä. Työssä tutkitaan ensin kapasitiivisten kytkentäelementtien optimaalista muotoilua ja sijoittamista. Seuraavaksi osoitetaan simulaatioin ja mittauksin, että matkapuhelimen antennirakenteen kaistanleveys-tilavuus-suhdetta saadaan parannettua huomattavasti käyttämällä optimoituja kytkentäelementtejä perinteisten resonanssityyppisten antennielementtien sijaan. Kytkentäelementteihin perustuvien moniresonanssi antennirakenteiden toteuttamisen helpottamiseksi työssä esitetään myös teoreettinen tutkimus ei-resonoivien kytkentäelementtien sovittamisesta kaksoisresonanssiin. Kytkentäelementtien soveltuvuutta monitaajuuspäätelaitteisiin havainnollistetaan uudentyyppisellä nelitaajuus-GSM-antennilla, jonka kokonaistilavuus on ainoastaan 0.7 cm^3. Lopuksi esitellään uudentyyppinen kytkentäelementeille suunniteltu taajuussäädettävä sovituspiiri.

Tässä työssä tutkitaan myös matkapuhelinantennien kaistanleveyttä, hyötysuhdetta puheasennossa ja SAR- (specific absorption rate) arvoja taajuuden funktiona laajalla taajuuskaistalla (0.6 GHz - 6 GHz) hyödyntäen kytkentäelementtejä. Tulokset osoittavat, että 3 GHz:n alapuolella näihin kolmeen parametriin vaikuttavat vahvasti rungon resonoivat aaltomuodot, kun taas 3 GHz:n yläpuolella kytkentäelementin aaltomuodot dominoivat. Yllä olevan lisäksi työssä tutkitaan taitettavan puhelimen rungon resonoivia aaltomuotoja kytkentäelementtien avulla. Tulokset tuovat esille useita haasteita, kuten säteilemättömän resonanssin, joita antennisuunnittelija saattaa kohdata taitettavien puhelinten kanssa.

Työn toinen osa keskittyy matkapuhelinten moniantennirakenteiden suorituskyvyn arviointiin. Ensin uudentyyppisen mittauksiin perustuvan antennien testialustan (MEBAT) tarkkuutta arvioidaan perusteellisesti. Tämän jälkeen useiden matkapuhelinten moniantennirakenteiden suorituskykyä tutkitaan järjestelmällisesti MEBATin avulla. Painotus on moniantennirakenteiden tehovastaanotto-ominaisuuksissa (effective array gain tai *EAG*). Työssä ehdotetaan tarkkaa ja nopeaa teoreettista tapaa antennirakenteen *EAG*:n mediaanin ennustamiseksi. Teoreettisten ja empiiristen *EAG*-tulosten perusteellisen analyysin pohjalta annetaan suosituksia moniantennijärjestelmän säteilykuvion optimaalisille ominaisuuksille. Tutkituissa MIMO-järjestelmissä saatujen ominaisarvohaje- ja kapasiteettitulosten perusteella tehdään johtopäätös, että matkapuhelimen antennisuunnittelun keinoin voi olla vaikeaa vaikuttaa MIMO-järjestelmän kykyyn muodostaa rinnakkaisia kanavia. Esitetyt tulokset ehdottavat, että matkapuhelimen antennisuunnittelijan tulisi pääasiassa keskittyä *EAG*:n maksimointiin.

Table of contents

List of Publications

This thesis is based on the work presented in the following papers.

[P1] J. Villanen, J. Ollikainen, O. Kivekäs, and P. Vainikainen, "Coupling element based mobile terminal antenna structures," *IEEE Transactions on Antennas and Propagation*, vol. 54, no. 7, pp. 2142 – 2153, July 2006.

[P2] J. Villanen and P. Vainikainen, "Optimum dual-resonant impedance matching of coupling element based mobile terminal antenna structures," *Microwave and Optical Technology Letters*, vol. 49, no. 10, pp. 2472 – 2477, October 2007.

[P3] J. Villanen, C. Icheln, and P. Vainikainen, "A coupling element based quad-band antenna structure for mobile terminals," *Microwave and Optical Technology Letters*, vol. 49, no. 6, pp. 1277-1282, June 2007.

[P4] J. Villanen, M. Mikkola, C. Icheln, and P. Vainikainen, "Radiation characteristics of antenna structures in clamshell-type phones in wide frequency range," *Proc. IEEE 65th Vehicular Technology Conference (VTC2007-spring)*, Dublin, Ireland, April 2007, CD-ROM (ISBN 1-4244-0266-2), pp. 382-386.

[P5] J. Villanen, J. Poutanen, C. Icheln, and P. Vainikainen, "A wideband study of the bandwidth, SAR and radiation efficiency of mobile terminal antenna structures," *Proc. International Workshop on Antenna Technologies Conference (IWAT'07)*, Cambridge, UK, March 2007, pp. 49-52.

[P6] P. Suvikunnas, J. Villanen, K. Sulonen, C. Icheln, J. Ollikainen, and P. Vainikainen, "Evaluation of the performance of multiantenna terminals using a new approach," *IEEE Transactions on Instrumentation and Measurement*, vol. 55, no. 5, pp. 1804 - 1813, October 2006.

[P7] J. Villanen, P. Suvikunnas, C. Icheln, J. Ollikainen, and P. Vainikainen, "Advances in diversity performance analysis of mobile terminal antennas," *International Symposium on Antennas and Propagation (ISAP'04)*, Sendai, Japan, August 2004, CD-ROM (ISBN 4-88552-208-0), paper 3A3-3.pdf.

[P8] J. Villanen, P. Suvikunnas, C. Icheln, J. Ollikainen, and P. Vainikainen, "Performance analysis and design aspects of mobile terminal multi-antenna configurations," *IEEE Transaction on Vehicular Technology*, to be published.

Author's contribution

In publications [P1]-[P6] and [P8], the author of this thesis had the main responsibility for preparing the papers. Professor Pertti Vainikainen supervised all the papers. Dr. Clemens Icheln instructed papers [P3]-[P8]. More details are given below.

In [P1], this author had the leading role in developing the entire paper. Dr. Jani Ollikainen and Dr. Outi Kivekäs participated in the work as instructors. Dr. Clemens Icheln assisted with radiation pattern measurements.

Paper [P2] is based on the idea of Prof. Pertti Vainikainen. This author made all the analytical derivations, conducted the simulations, as well as prepared the paper.

The antenna structure presented in [P3] was invented by this author. This author designed and measured the prototype antenna, and had the leading role in preparing the paper. Dr. Clemens Icheln assisted with radiation pattern measurements.

Paper [P4] is partly based on the ideas emerged from the master's thesis of Milla Mikkola, in which this author worked as an instructor. This author conducted all the simulations reported in [P4], and had the main responsibility for preparing of the paper. Milla Mikkola participated in the analysis of the results and in the writing of the paper. The frequency tunable matching circuitry presented in [P4] was invented and analysed by this author.

This author defined the work done in [P5], and was responsible for calculations of bandwidth potentials. In addition, this author simulated the studied antenna structures in free space. Juho Poutanen was responsible for SAR and radiation efficiency simulations in talk position. Analysis of the results and writing of the paper was carried out in co-operation by this author and Juho Poutanen.

This author participated in the development and validation work of the analysis tool (MEBAT) studied in [P6]. Main part of the development work of the tool was carried out by Dr. Pasi Suvikunnas and Dr. Kati Sulonen. This author also participated in preparing of the manuscript.

In [P7], this author carried out all the simulations with the measurement based antenna test bed (MEBAT). This author also had the main responsibility for the analysis of the results as well as preparing of the paper. The diversity antenna configurations studied in [P7] were designed by Dr. Jani Ollikainen. Their radiation patterns, efficiencies and S-parameters were simulated by Dr. Jani Ollikainen and Dr. Clemens Icheln.

In [P8], this author carried out all the SIMO system simulations with the measurement based antenna test bed (MEBAT). This author also had the main responsibility for the analysis of the results as well as preparing of the paper. The diversity antenna configurations studied in [P8] were designed by Dr. Jani Ollikainen. Their radiation patterns, efficiencies and S-parameters were simulated by Dr. Jani Ollikainen and Dr. Clemens Icheln. The MIMO system simulations were carried out by Dr. Pasi Suvikunnas.

1 Introduction

1.1 BACKGROUND

The rapid evolution of wireless communications systems and terminal devices has made the implementation of small multi-band antennas one of the main technical challenges. The number of wireless systems in which multimode mobile terminals are required to operate has been growing constantly in recent years. As each wireless system needs an antenna and typically also its own frequency band to operate, there has been a pressure to increase the volume reserved for the antennas inside a mobile terminal. Possible use of multi-antenna reception, e.g. in MIMO (Multiple-Input Multiple Output) systems, further increases the pressure. At the same time, the trend in the market has been to decrease the size, especially the thickness, of the terminal devices. The requirements set for antenna design are therefore contradictory; the size of an antenna should be decreased while increasing its performance.

It has been known already for some time that the performance of a small antenna element is strongly affected by the metallic chassis of a mobile terminal. The antenna element excites currents on the chassis, which works as an important part of the antenna structure. In order to achieve the maximum relative bandwidth available with an antenna element having a certain size, it is essential that the antenna element excites the radiating wavemodes of the chassis as strongly as possible. In fact, the presence and usage of the chassis as part of the antenna structure has made the implementation of current low-volume antenna elements possible; the maximum dimensions allowed for an internal antenna element are typically so small that the bandwidth requirements set for modern mobile terminals cannot be met with the resonant modes of a small antenna element alone.

Short-circuited patch-type antennas, like planar inverted-F antennas (PIFA), are commonly used as internal antennas in modern mobile terminals. The antenna elements are typically self-resonant, i.e. impedance matching is built-in into the metallic structure of the antenna element. With self-resonant antenna elements it is difficult to achieve optimum coupling to the wavemodes of the chassis, as typically only part of the volume occupied by the antenna element effectively contributes to coupling. To address the problem, self-resonant antenna elements have been suggested to be replaced with non-resonant coupling elements. The idea is to select the shape, type, and location of the coupling element so that coupling to the dominant wavemodes of the chassis is maximized within the used volume. Impedance matching to the transceiver electronics at the desired frequency is done with a separate matching circuitry. Before optimized multi-resonant and multi-band antennas can be realized by using the idea of coupling elements, in-depth knowledge is required on the optimum tuning and implementation of not only the coupling elements but also the matching circuits.

When a significant part of radiation is originated from the wavemodes of the chassis, it can be expected that the performance of the antenna structure is strongly affected by the presence of the nearby user's lossy tissues, such as the head and hand. A comprehensive understanding on the combined performance of the antenna, chassis, and the user is thus needed to optimize antenna performance. Profound knowledge of the behavior of the resonant wavemodes of the chassis is especially important when designing antennas for clamshell-type phones, in which the electrical properties of the chassis depend strongly on the mechanical use position of the phone, i.e. whether the phone is open or closed.

In addition an internal antenna should be small in size and have high efficiency over wide frequency bands, it must also be able to provide reliable power transmission in real multipath propagation environments. Due to multipath propagation, the signal power arriving at the mobile consists of multiple components, each having its distinctive angle of arrival, phase, and amplitude. When the mobile terminal moves, the relative phases of the multipath components change, which causes rapid variations and deep fades, i.e. fast fading, in the envelope of the total received signal. A well-known way to mitigate the effects of fast fading is to use multi-antenna, i.e. diversity reception in the mobile terminal. In MIMO systems, multiple antennas are additionally used at the base station, which together with spatial multiplexing offers the possibility for significantly improved spectral efficiencies. In both cases, fast and reliable methods are needed for the performance evaluation of multi-antenna terminals. The performance of an antenna configuration should be investigated not only under realistic channel conditions, but also in a realistic use position of the device, such as in talk position beside the user's head and hand.

1.2 OBJECTIVES OF THE THESIS

The general objective of this thesis is to provide novel and useful information for the design of mobile terminal antenna structures. The work has been divided into two parts. The main objective of the first part is to increase general understanding of the main benefits, drawbacks and application areas of coupling element based mobile terminal antenna structures, with special attention paid to antenna miniaturization. The purpose is also to improve understanding of the combined performance of a small antenna and the chassis of a monoblock- or clamshell-type mobile terminal. One of the objectives of the second part of the thesis is to evaluate the accuracy and usability of a novel measurement based antenna test bed (MEBAT). A further aim is to identify the properties of a multi-antenna configuration that are important for the performance obtained in real propagation environments, as well as to develop fast and accurate theoretical ways of predicting the antenna performance.

1.3 ORGANIZATION OF THE THESIS

In the first part of this thesis [P1]-[P5], the main benefits, drawbacks and application areas of coupling element based mobile terminal antenna structures are studied. Papers [P1]-[P4] consider the miniaturization and performance enhancement of mobile terminal antennas. The effect of the chassis of a mobile terminal on various important antenna-related parameters is studied in [P4],[P5]. The second part of the thesis [P6],[P7],[P8] concentrates on performance evaluation of mobile terminal multi-antenna configurations. A novel measurement based antenna test bed (MEBAT) is presented and its accuracy is thoroughly evaluated in [P6]. In papers [P7],[P8], the performance of several mobile terminal multi-antenna configurations are thoroughly investigated using MEBAT.

The summary part of the thesis is organized in the following manner. Chapter 2 presents briefly the fundamentals of mobile terminal antennas. The optimum shaping, placement, and impedance matching of coupling elements, as well as their main benefits and drawbacks, are considered in Chapter 3. Chapter 4 deals with implementation techniques of coupling element based multi-band and multi-resonant antennas. Radiation characteristics of mobile terminal antennas are analyzed over wide frequency range in Chapter 5. Chapter 6 concentrates on performance evaluation of mobile terminal multi-antenna configurations. Summaries of publications [P1]-[P8] are presented in Chapter 7 and conclusions are given in Chapter 8.

2 Mobile terminal antennas

2.1 INTRODUCTION

One of the trends in mobile communications industry has been to significantly decrease the size of mobile terminals. Meanwhile, the number of radio systems and thus frequency bands in which mobile terminals are required to operate is growing steadily. This development has set urgent need for internal low-volume and low-profile antenna structures being able to operate efficiently in a number of frequency bands. Miniaturization of an already small antenna, however, is not a straightforward task. It has been known already for decades that the electrical size of a small antenna cannot be decreased arbitrarily without its other important properties, like bandwidth and efficiency, being affected [1]-[4].

The PCBs (Printed Circuit Board) of today's mobile terminals have usually continuous ground layers on their both sides. In addition, planar metal surfaces are commonly used inside mobile terminals as EMC (Electromagnetic Compatibility) shields. The amount, size, and locations of the EMC shields can vary from phone to phone. The combination of the grounded PCB and the other metal layers form a solid few millimeters thick metal chassis, whose length and width roughly correspond to those of the PCB. It has been known already for long time that the metal chassis of a portable device has a significant effect on the performance of an antenna element mounted in the vicinity of it [5]. The antenna element couples currents to the chassis, which in consequence works as part of the antenna structure. Understanding of the interaction between a small resonant antenna element and the chassis of a mobile terminal has become an essential requirement for antenna designers.

The purpose of this chapter is to give the reader basic understanding of the fundamentals of mobile terminal antennas. The antenna technologies used in current multi-band mobile terminals are reviewed later in Chapter 4. In this chapter, first some of the most important terms related to mobile terminal antennas are briefly presented. This is followed by discussion on fundamental limitations related to antenna size reduction. Finally, radiation mechanism of the combination of mobile terminal antenna and chassis is discussed.

2.2 FUNDAMENTAL TERMS

2.2.1 Quality factor

An important parameter specifying the frequency selectivity of an antenna is quality factor, or Q. A general definition of Q that is applicable to any resonant system is [6]

$$Q = \omega_r \frac{W}{P_l} = 2\pi f_r \frac{W}{P_l}, \tag{2.1}$$

where ω_r is angular resonant frequency, f_r is resonant frequency, W is total time-average energy stored in the system, and P_l is power loss per second in the system. Several different quality factors can be defined for an antenna. The so-called unloaded quality factor (Q_0), which is computed by including only the internal losses of an antenna in the denominator of Eq. (2.1), is an important metric for an antenna designer. The internal losses of an antenna can

be divided into radiation, dielectric, and conductor losses, which can be further described by radiation (Q_r), dielectric (Q_d), and conductor (Q_c) quality factors, respectively.

2.2.2 Impedance bandwidth

In case of mobile terminal antennas, the term bandwidth typically refers to impedance bandwidth. Impedance bandwidth is usually defined as the frequency range, within which reflection coefficient (S_{11}) at the antenna input stays below a certain predefined level. In recent years, $S_{11} \leq$ -6 dB (return loss $L_{retn} \geq$ 6 dB) has become a widely used matching criterion for low-volume internal antennas in mobile terminals. In practice, the matching criterion is set according to the requirements of the wireless communications system at hand. It can be shown that the relative impedance bandwidth (B_r) of a resonant circuit describing an antenna is inversely proportional to its unloaded quality factor (Q_0) [7],[8].

2.2.3 Efficiency

The losses of an antenna can be characterized by radiation and total efficiencies. Radiation efficiency (η_r) is defined as the ratio of the power radiated (P_r) by an antenna to the input power accepted (P_{in}) by the antenna, and can also be expressed in terms of the unloaded and radiation quality factors of the antenna:

$$\eta_r = \frac{P_r}{P_{in}} = \frac{Q_0}{Q_r}. \qquad (2.2)$$

Often the antenna structure of a mobile terminal is simply modeled as the combination of an antenna element and a metal chassis. In free space, the radiation efficiency of this kind of a fully metallic prototype can be larger than 95 % over the frequency bands of the E-GSM900, GSM1800, PCS1900 and UMTS systems [9]. In real mobile terminals, free space radiation efficiencies are significantly lower as the battery, display, loudspeaker, plastic covers, and other lossy parts of the terminal absorb part of the antenna input power. A significant part of the antenna input power can be additionally lost to the user's head, hand, and other body parts typically located in close proximity to a mobile terminal. In [10] and [11], the radiation efficiencies of five commercial dual-band phones were studied by measurements in free space and in talk position with 15 test persons holding the phones next to their heads. In free space, radiation efficiencies of 54-80% and 32-72% averaged over the E-GSM900 and GSM1800 bands were reported, respectively. In talk position, average radiation efficiencies of 6-9% and 6-13% were reported for the E-GSM900 and GSM1800 bands, respectively.

Radiation efficiency does not take into account the reflection losses occurring at the input of an antenna. The so-called total efficiency includes also reflection losses, i.e. it describes how much of the power available at the feed of an antenna is converted into radiated power. A return loss of L_{retn} = 6 dB at antenna input, for example, means that the power accepted by the antenna (P_{in}) is reduced by 25 % compared to a perfectly matched antenna.

2.2.4 Specific Absorption Rate (SAR)

Specific Absorption Rate (*SAR*) is a parameter that is used to evaluate the radio frequency (RF) energy absorbed by human tissue. It is expressed in units of watts per kilogram (W/kg) and is defined by

$$SAR = \frac{\sigma \cdot |E_{rms}|^2}{\rho}, \tag{2.3}$$

where E_{rms} is the root mean square (rms) value of the electric field strength (V/m) in the tissue, σ is the effective conductivity of the tissue (S/m), and ρ is the density (kg/m^3) of the tissue. Several regulatory agencies have set mandatory safety limits for the *SAR* values caused by mobile terminals [12],[13]. These limits are based on the RF exposure recommendations given in [14],[15], see Table 2.1. Standard practices for evaluating the *SAR* compliance of mobile terminals are described in [16]-[18].

Table 2.1, *RF exposure recommendations given by IEEE/ANSI [14] and ICNIRP [15].*

	IEEE/ANSI	**ICNIRP**
SAR [W/kg] in body except hands, wrists, feet, ankles (averaging mass)	1.6 (1 g)	2.0 (10 g)
SAR [W/kg] in hand, wrists, feet, ankles (averaging mass)	4 (10 g)	4 (10 g)
Volume shape	Cube	Any of 10 g contiguous tissue
Averaging time [min]	30	6
Whole body averaged SAR [W/kg]	0.08	0.08

Specific Absorption Rate is an important topic for antenna designer for two reasons. On one hand, an antenna designer needs to make sure that a mobile terminal complies with *SAR* standards. On the other hand, *SAR* provides a valuable insight on the power absorbed by the user. Minimizing *SAR* and thus user interaction improves the radiation efficiency and thus the overall performance of a mobile terminal in use position.

Currently there exist two competing theories, [19] and [20], on the interaction mechanism between a biological tissue and the near fields of an antenna. The first one [19] claims that the surface currents induced by the magnetic near fields of an antenna to a human tissue are the main power dissipation mechanism, while coupling from electric near fields is of less importance. Based on simulations with dipole antennas operating above 300 MHz, it is concluded in [19] that SAR in the human tissue is roughly proportional to the square of the magnitude of antenna current. These conclusions, however, are not fully supported by the results of a related study [21]. In [21], the SAR generated by a dipole antenna located beside a homogeneous muscle phantom with and without a covering fat layer was studied at 915 MHz. Without the fat layer, the SAR maximum was located on the surface of the muscle near the antenna feed point, i.e. on the maximum of magnetic field. With the fat layer, however, SAR maxima were found from the surface of the fat layer under the open ends of the dipole.

In [20], the electric near fields and SAR generated by a dipole antenna located beside several different compositions of tissues were studied at 900 MHz. The results lead to the conclusion that the location of peak SAR is actually not related to the maximum of antenna currents. Instead, the location of the SAR maxima can be explained by applying electric field boundary conditions with the electric near field components parallel and perpendicular to the surface of the tissue [20]. With tissues having high permittivity (like muscle or skin) the field components perpendicular to the surface of the tissue are attenuated substantially. In case of a dipole antenna, SAR maximum can be consequently found from a location with low original total electric fields but with significant components parallel to the surface of the tissue, i.e. from the surface of the tissue near the center point of the dipole [20]. With low-permittivity tissues, such as fat, SAR maxima are found from the locations of high original total electric fields, i.e. from the ends of the dipole, as the perpendicular field components are not considerably attenuated according to boundary conditions [20].

2.3 FUNDAMENTAL LIMITATIONS ON ANTENNA SIZE REDUCTION

It is a commonly known fact that the radiation quality factor (Q_r) and thus the bandwidth of an antenna are ultimately limited by the electrical size of the antenna [1]-[4],[22]-[26]. A theory on the minimum radiation quality factor achievable with an ideal linearly polarized antenna constrained to fit within a sphere of radius r, having no reactive energy stored inside, was first derived in [2]. The theory was extended in [3] to include also circularly polarized antennas. The lowest possible Q_r for a linearly polarized antenna is obtained when only the lowest order TM_{01} or TE_{01} mode is excited by the ideal antenna [2]. Theoretical fundamental minimum Q_r for this kind of an antenna structure can be expressed as [22],[25]:

$$Q_r = \frac{1}{(kr)^3} + \frac{1}{kr}, \tag{2.4}$$

where k is the wave number ($k = 2\pi/\lambda_0$, where λ_0 is free space wavelength) and r is the radius of the smallest sphere enclosing the antenna. According to Eq. (2.4), the Q_r of an ideal electrically small linearly polarized antenna is approximately inversely proportional to the volume V of the antenna in wavelengths (V/λ_0^3). The bandwidth of the antenna thus decreases rapidly when its electrical size is decreased.

In the derivation of Eq. (2.4), it is assumed that the antenna structure stores no reactive energy inside the sphere. In practice, antennas never completely fill the spherical volume enclosing them and also excite higher order wavemodes. In consequence, non-propagating energy is stored also inside the enclosing sphere, which inevitably increases the Q_r and thus decreases the bandwidth of the antenna [3],[25].

2.4 THE COMBINATION OF MOBILE TERMINAL ANTENNA AND CHASSIS

2.4.1 General

Self-resonant IFAs (Inverted-F Antenna) [27], PIFAs (Planar Inverted-F Antenna) [5], and different variants of these are currently the most common internal antenna technologies used in mobile terminals. The maximum dimensions allowed for internal antenna elements are typically so small that the bandwidth requirements set for modern mobile terminals cannot be

met with the resonant modes of the antenna elements alone. Obviously, some help is needed from a larger metallic object, which is provided by the chassis of a mobile terminal. In fact, it was shown already in [28] that the radiation resistance and efficiency of a small antenna can be significantly increased by using the antenna as a probe to excite currents on a larger metallic object with lower Q_r.

The first step towards understanding the contribution of the chassis of a mobile terminal on the performance of an internal antenna element was made in [5]. The results indicated that the impedance bandwidth of a PIFA reaches its maximum when the electrical length of the chassis equals roughly $0.4\lambda_0$, i.e. when the chassis is at its half wave resonance. After [5], a considerable number of papers aimed to clarify the interaction between a small resonant antenna element and the chassis of a mobile terminal have been published [29]-[40]. The results show that the impedance bandwidth [29]-[37], talk position efficiency [37],[38], *SAR* [33],[37]-[39], and radiation pattern shape [33],[40] of this combination depend not only on the electrical characteristics of the antenna element, but also strongly on the dimensions of the chassis and the position of the antenna element relative to it. Comprehensive review and analysis of the results published in [5],[29]-[40] can be found in [41],[42]. In the rest of this thesis, the results of [5],[29]-[40] are referred and discussed whenever necessary.

The so-called resonator based analysis, first used in [31],[35] and later applied in [43], provides a useful circuit-theoretical tool for the analysis of the combined performance of a single-resonant antenna element and a chassis. In order to fully understand the behavior of the combination of antenna and chassis, it is essential that one has good understanding on the radiation and resonance characteristics of the chassis. A useful tool for that purpose is provided by the so-called characteristic mode theory [44],[45]. In the following sections, the resonator based analysis and characteristic mode theory are shortly introduced and some of the most important results found from the open literature are briefly reviewed.

2.4.2 Resonator based analysis

In the resonator based analysis [31],[35], it is assumed that waves in the combination of antenna and chassis can be divided into two fairly independent resonant wavemodes; the quasi-TEM wavemode of a typical self-resonant antenna element, and the thick-dipole type wavemode of a chassis. These resonant wavemodes can be modeled as two coupled lumped element resonant circuits, whose properties can be further described by their respective resonant frequencies and unloaded quality factors. The strength of coupling between the wavemodes is described by an ideal transformer placed between the resonators.

At 900 MHz, according to [35], a small self-resonant antenna element like PIFA radiates typically only about 10 % portion of the total power radiated by a mobile terminal. The rest of the power is radiated by the half-wave dipole-type current distribution of the chassis. At 1800 MHz, the contribution of the antenna element wavemode is clearly larger, roughly 50 %. In addition to the above, it was shown in [35] that the maximum bandwidth achievable with the combination of antenna and chassis remains almost unaffected when the unloaded quality factor of the antenna element is increased from $Q_0 = 20$ to $Q_0 = 500$. When the antenna element becomes more and more narrowband, however, a stronger coupling to the chassis wavemode is needed to reach the maximum relative bandwidth, which is obtained with an optimally coupled dual-resonant response [35]. The above-described results were obtained by

assuming that the resonant frequencies of the antenna element and chassis are equal. In practice, the optimum case of equal resonant frequencies may not be realizable. The first order ($\lambda/2$) resonance of a chassis with typical dimensions of 100 mm x 40 mm (length x width) is located roughly at 1.1 GHz [35], which is outside the operating bands of current communications systems. In [43], it was shown that also at operating frequencies below first chassis resonance, like at the E-GSM900 band (880 MHz – 960 MHz), the maximum achievable relative bandwidth is not limited by the unloaded quality factor of the antenna element.

2.4.3 Characteristic mode theory

The theory of characteristic modes for conducting bodies [44],[45] provides a useful field-theoretic method for characterization of chassis wavemodes. Currents on the surface of a conducting body can be expanded into characteristic modes. Each mode is associated with a set of eigenvalues, whose magnitude depicts how well the particular mode radiates. Based on the eigenvalues, it is possible to numerically evaluate the radiation quality factors associated with each characteristic mode [46]. The resonant frequency of a certain characteristic mode can be easily obtained from the frequency response of its eigenvalues. In [47], the first eight characteristic modes of a rectangular plate with dimensions 40 mm x 60 mm were presented and analyzed. Later in [46],[48]-[50], the method was applied to study the radiation properties of typical-sized (100 mm x 40 mm) mobile terminal chassis. In [46], radiation quality factors of 2.3, 3.0, 2.5, and 2.3 were reported for the first four characteristic modes of the chassis excited with a plane wave. The respective resonant frequencies of the modes were 1260 MHz, 2679 MHz, 2739 MHz, and 3081 MHz. The first two modes represent the major axis half- and full-wave dipole modes of the chassis. The third mode represents the minor axis half-wave mode of the chassis, whereas the fourth mode represents magnetic dipole mode [46]. In practice, currents on the chassis of a mobile terminal at a given frequency are superposition of these modes. At lower frequencies, the half-wave dipole-type mode of the chassis is clearly dominant [46]. One should note that excitation of the modes is largely dependent on the type and location of the exciting element. A patch-type antenna element placed on top of the shorter end of a chassis, for example, can efficiently excite only the major axis dipole modes of the chassis.

3 Coupling element based mobile terminal antennas

3.1 INTRODUCTION

The results published in [35] indicate that especially below 1 GHz, like at the E-GSM900 band, the antenna element of a mobile terminal works mainly as a matching element, which excites the low-Q wavemodes of the chassis. To achieve the maximum available relative bandwidth with an antenna element of a certain size, it is essential that the antenna element couples as strongly as possible to the dominant wavemode of the chassis [35].

Short-circuited patch-type antennas, like PIFAs, are commonly used in modern mobile terminals. Impedance transformation and resonance tuning are built-in into the metallic structures of these self-resonant antenna elements. This enables e.g. low production costs and easily obtained matching. On the other hand, it can be difficult to achieve optimum coupling to the dominant wavemode of the chassis, as typically only part of the volume occupied by a shorted self-resonant antenna element effectively contributes to coupling.

In [31],[35],[51], a novel idea was proposed to address the problem. It was suggested that the size of an internal antenna could be considerably reduced by replacing a self-resonant antenna element with an essentially non-resonant coupling element, whose main purpose is to efficiently excite the wavemodes of the chassis. Separate matching circuitry is used to tune the combination of coupling element and chassis into resonance at the desired operating frequency. As the coupling element is a separate unit from impedance matching functionality, its shape, size and location can be optimized individually to achieve the strongest available coupling to the dominant wavemode of the chassis.

The main purpose of this thesis, inspired by [31],[35],[51], was to increase general understanding on the optimum tuning and design, as well as on the main benefits and drawbacks of coupling element based antenna structures. The work started with a thorough and systematic investigation of the idea of coupling elements [P1], and continued with a theoretical study on optimum dual-resonant impedance matching of coupling elements [P2]. This chapter presents the main findings of [P1],[P2], but also other related studies available from open literature are referred whenever necessary. Coupling element based multi-band and multi-resonant antenna structures [P2],[P3],[P4], and other application areas of coupling elements [P4],[P5] are discussed in Chapters 4 and 5, respectively.

3.2 OPTIMUM SHAPE AND LOCATION OF A COUPLING ELEMENT

The wavemodes of a chassis can be excited either via the magnetic or the electric fields of the chassis, or optionally, with direct galvanic contact to separated parts of the chassis [51]. Patch-type antenna (or coupling) elements couple mainly capacitively, i.e. via electric fields. Maximum coupling requires that electric fields of the chassis and of the exciting element are oriented in parallel. It is also important that electric field maxima of the chassis and the exciting element are co-located. Patch-type coupling elements have been studied e.g. in [35],[51]-[55],[P1]-[P5]. Coupling via magnetic fields is possible e.g. with an inductive loop arranged so that its magnetic field coincides with that of the chassis wavemode, as demonstrated in [52],[56]. Excitation of chassis wavemodes with a direct galvanic contact,

e.g. with a feed placed over an impedance discontinuity on a chassis, such as a slot, has been demonstrated e.g. in [57],[58].

In order to achieve the maximum bandwidth available with an antenna or coupling element having a certain unloaded quality factor, it is essential that the element is shaped and located such that coupling to the nearest resonant wavemode of the chassis is maximized. In [P1], the optimum shape and location of a coupling element were systematically studied with IE3D simulations by moving a small capacitive probe (height = 3mm, diameter = 2 mm) on top of a chassis with dimensions 100 mm x 40 mm x 3 mm (height x width x thickness). From IE3D simulation data, unloaded quality factors were calculated for each probe location at 920 MHz and 1800 MHz. Fig. 3.1 presents the simulation setup and the normalized quality factors obtained at 920 MHz with a probe moved on top of the plane A of the chassis.

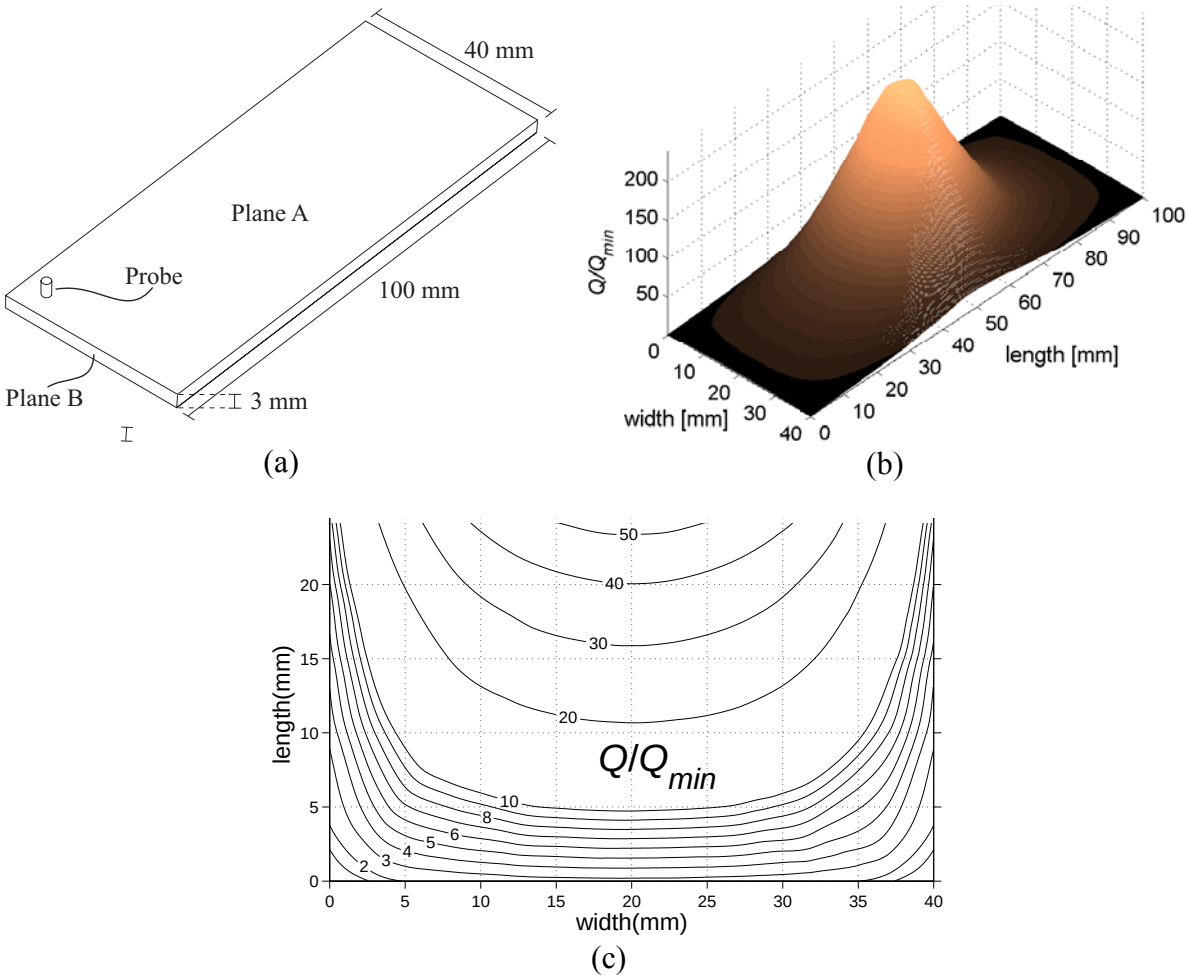

Figure 3.1. *(a) Simulation setup. (b) A 3-D view on the simulated normalized (Q_{min} = 195 at the corners of the chassis) unloaded quality factors obtained at 920 MHz when the probe has been moved on top of plane A, and (c) a closer view on a shorter end of the chassis [P1].*

Before interpreting the results shown in Fig. 3.1, it is useful to understand the behavior of the electric near fields of chassis wavemodes. The chassis of a mobile terminal supports dipole-type wavemodes, which are resonating when the electrical length of the chassis is a multiple of $\lambda/2$ at the operating frequency. At the $\lambda/2$ resonance of a chassis, for example, current

distribution minima and thus electric field maxima are located at the ends of the chassis. Respectively, current distribution maximum and thus electric field minimum is located at the center of the chassis [35],[46], like in a half-wave dipole. In [50], electric near fields of the half-wave dipole mode of a chassis were further studied with help of the characteristic mode theory. The results revealed that the intensity of electric near fields, computed at a distance of 5 mm above the surface (plane A in Fig. 3.1 (a)) of a chassis, reaches its maximum on top of the corners of the chassis. The above-described findings fully explain the results shown in Fig. 3.1. When the probe is moved on top of the plane A of the chassis, the strongest coupling and thus the lowest quality factors are achieved on top of the shorter ends of the chassis. Respectively, the weakest coupling is obtained on top of the center of the chassis. Quality factor reaches its minima on top of the corners of the chassis, as expected.

In addition to the above, results obtained with a probe moved on top of the plane B of the chassis were briefly reported in [P1] (see [52] for numerical results). Very strong coupling was obtained in the whole area of the plane B, with maxima again at the corners of the chassis. As shown in [46] and [50], electric near fields at the ends of a chassis are oriented mostly in parallel with the longitudinal axis of the chassis. In order to couple to these electric fields optimally, a coupling element should be extended outside the top perimeter of a chassis and bent perpendicularly towards the plane A [P1]. A more complete illustration will be provided later in this thesis (Figs. 3.4 and 4.1). A similar technique to increase coupling to the wavemodes of chassis has been demonstrated with self-resonant PIFA-type antenna elements in [31],[35].

Based on the above discussion, it can be suspected that the structures of many planar self-resonant antennas, like IFAs and PIFAs, are not optimal. First of all, currents are typically very high near the shorting pins of these antenna elements. In consequence, electric fields near the shorting pins are weak, as shown e.g. in [59],[60]. This results in reduced coupling between the wavemodes of the antenna element and the chassis. Furthermore, to keep the dimensions of self-resonant multi-band antennas compact, some kind of meandering of the antenna parts used for low-band (like E-GSM900) operation is typically needed [9],[59],[61],[62]. Due to meandering, optimum shaping of the important parts of the antenna element according to the high-coupling locations of the chassis can become difficult. A comprehensive comparison between coupling element based antenna structures and traditional self-resonant PIFA based antenna structures will be presented later in this chapter.

3.3 IMPEDANCE MATCHING NETWORKS

3.3.1 General

After a coupling element is shaped and located optimally in the vicinity of a chassis, it needs to be matched at the desired operating frequency with a separate matching network. Matching of a complex load into single or higher order resonance can be done in various ways by using the well-known impedance matching principles described e.g. in [63]. When selecting the implementation technique of the matching network, attention has to be paid on such important aspects as the ohmic losses, complexity, tolerances, price, and PCB area consumption of the final implementation.

Modern high-Q discrete components offer a feasible way of implementing matching circuitries with low losses and compact size. Distributed components, realized e.g. by microstrip or coplanar lines, can be naturally used as well. The third option is to utilize recent advances in integration technology. With multi-layer LTCC (Low-Temperature Co-fired Ceramic) substrates, a large number of high-Q inductors, capacitors, transmission lines, and other passive elements can be integrated into a single package having an extremely low volume and high efficiency [64]-[66]. Moreover, integrating matching circuitry with the front-end module of a mobile terminal, which is usually LTCC-based, should have only minor implications on the production time, costs, and PCB area consumption.

In this section, theoretical limitations on broadband impedance matching of complex loads are first presented. After this, the principles of matching non-resonant antenna structures into single-resonance are briefly discussed. Finally, the theory and methodology of matching non-resonant antenna structures optimally into dual-resonance are described.

3.3.2 Theoretical limitations on broadband impedance matching

At the frequency bands of current cellular systems, the input impedance of a coupling element is usually clearly capacitive and its real part is fairly low [P1],[P2]. In an ideal case, the matching network would transform the complex input impedance of the coupling element to purely resistive, e.g. to 50 Ω, over all desired frequency bands. This is, however, not possible in practice, as there exist fundamental limitations on broadband impedance matching [67],[68]. The results of [68] show that it is not possible to match an arbitrary impedance to a pure resistance over the whole spectrum, or even at all frequencies within a finite frequency band, by means of a purely reactive passive network. On the other hand, a perfect match can be obtained at a finite number of frequencies. Making reflection coefficient very small at any point of the pass band, however, leads to a reduction of theoretical maximum bandwidth [68]. Therefore, it is often better to accept less than a perfect but still good matching in the whole pass band. The level of tolerance can be defined e.g. in terms of the minimum allowed return loss (L_{retn}).

Let us now assume that the non-resonant coupling element has been tuned into single-resonance with an appropriate reactive component. A well-known and effective way of increasing the impedance bandwidth of a resonator is to add more resonances into its frequency response [67],[68]. This can be obtained with a matching network consisting of one or more high-Q matching resonators. The improvement in bandwidth, however, saturates rapidly as the number of matching resonators increases. With only one matching resonator (n = 2), already roughly 60 % of the maximum bandwidth is obtained [41]. With five matching resonators, roughly 90 % of the maximum bandwidth is achieved [41], but also the ohmic losses and the design complexity of the matching network are obviously higher.

3.3.3 Single-resonant impedance matching

In order to match the combination of coupling element and chassis into a critically coupled (perfect match at f_r) single-resonance, one needs to a) cancel the antenna structure's input reactance at f_r, and b) transform the antenna structure's input resistance to 50 Ω at f_r. Both of these functions can be simultaneously accomplished with a simple L-section matching network consisting of two lumped or distributed elements of the suitable value and type.

Explicit design equations can be found e.g. from [63]. In practice, a perfectly matched, i.e. critically coupled, antenna does not provide an optimum bandwidth. The maximum bandwidth is achieved with a slightly over-coupled antenna, as described in [8]. The theoretical relative bandwidth of an optimally over-coupled single-resonant antenna having a certain Q_0 can be expressed as (by combining Eqs. (6) and (8) in [8])

$$B_{sr,opt} = \frac{S^2 - 1}{2SQ_0}, \tag{3.1}$$

where S represents the maximum allowed voltage standing wave ratio.

3.3.4 Dual-resonant impedance matching

Background

In theory, the bandwidth achievable with an optimally coupled dual-resonant antenna having one high-Q matching resonator can be up to 2.1 times as large as the bandwidth achievable with an optimally over-coupled single-resonant antenna ($L_{retn} \geq 6$ dB) [41]. Dual-resonant matching thus provides an effective way of increasing the impedance bandwidth of a single-resonant antenna. The first question to ask is how to design a matching network providing an optimum dual-resonant response for a connected resonant or non-resonant antenna. An antenna designer would especially benefit from simple, explicit design equations.

Traditional filter and matching network design theory [63] usually aims to provide a perfect impedance matching at a number of frequencies in the pass band, which leads to a reduction of maximum obtainable bandwidth, as shown by [67],[68]. In [68],[69], design procedures were presented for matching networks producing an optimum band pass Chebyshev response of the desired order for a connected RLC load. For finding optimum circuit parameters, however, the graphical curves presented in [68],[69] are required. In [70], explicit formulas for the synthesis of optimum band pass Butterworth and Chebyshev impedance-matching networks were presented. The formulas, however, are fairly complex and the analysis applies only for a specific type of load consisting of an inductor in series with the parallel combination of a resistor and a capacitor. The so-called Simplified Real-Frequency Technique (SRFT) introduced in [71] offers one approach for pursuing optimum dual-resonant matching, but it is computationally fairly complex and does not provide an exact solution. Nevertheless, SFRT has proven to work well in broadband matching of antennas [72],[73].

Explicit design equations for matching networks designed to tune resonant antenna structures optimally into dual-resonance have been derived in [74]-[76] and as part of this work in [P2], respectively. The analysis of [P2] differs from the previous papers [74]-[76] in that it provides design procedures for matching networks which are particularly optimized for non-resonant coupling element based antenna structures. In [P2], special emphasis has been put on minimizing the complexity, i.e. component count, of the final matching network. This has been accomplished by properly choosing the type of the matching resonator, the location of impedance transformer, and the way how the non-resonant load is tuned into single-resonance. These aspects have not been considered in [74]-[76].

Tuning of a non-resonant load optimally into dual-resonance

Fig. 3.2 presents a schematic of the matching network used in [P2] to tune a non-resonant antenna structure, such as the combination of coupling element and chassis, optimally into dual-resonance. Resonator 2 in Fig. 3.2 represents the combination of a coupling element and chassis, tuned into resonance with two lumped elements of suitable value and type (inductor L_T and reactance X_m). As indicated by the results of [P2], the input impedance of a typical non-resonant coupling element can be with a good accuracy described as a series-resonant circuit. Thus, Resonator 2 can be considered to be of series-type. A series-resonant circuit can be tuned into dual-resonance by connecting a shunt parallel-type matching resonator into its feed [63]. Alternatively, a series-type matching resonator connected via an impedance inverter can be used [63], as shown in Fig. 3.2. As the input resistance of a coupling element is usually very low at cellular frequencies, typically less than 10 Ω, impedance transformation is additionally needed. In [P2], impedance transformation (an inversion) is accomplished right after Resonator 2. This way, discrete-component realization of the transformer can be almost completely integrated within the matching circuitry.

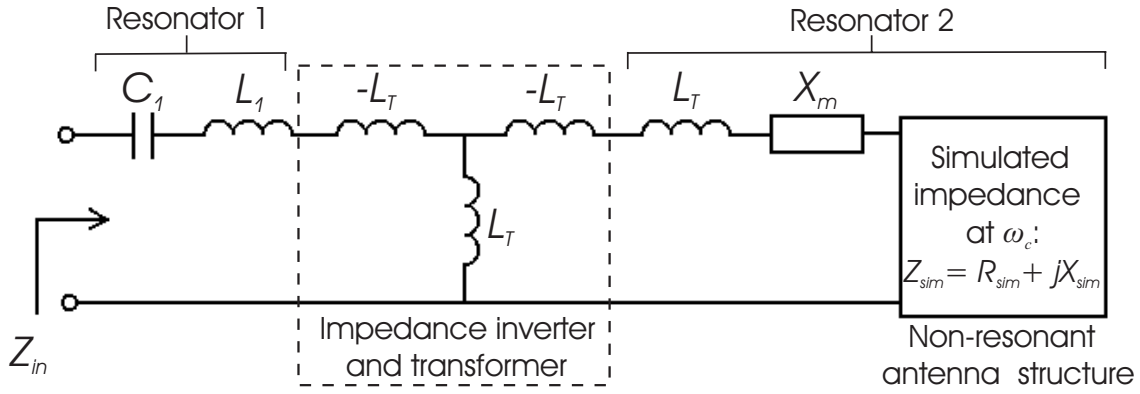

Figure 3.2. *Schematic of the matching network used to tune a non-resonant antenna structure optimally into dual-resonance. The block on the right represents the simulated input impedance (Z_{sim}) of the non-resonant antenna structure at the angular matching center frequency (ω_c) [P2].*

The inverter-transformer can be conveniently realized as a lumped element T-circuit consisting of positive and negative inductors [63], as illustrated in Fig. 3.2. An alternative implementation is obtained by replacing the inductors with capacitors [63]. In an ideal case, the negative components of the inverter-transformer can be absorbed into adjacent positive series components of the same type, so as to give a resulting circuit having all positive elements and minimum circuit complexity. The right-hand side negative component of the inverter-transformer can be absorbed by adding a positive component of the same value (L_T) into Resonator 2. Resonator 2 can be after this tuned into resonance with a reactance X_m, which is realized either as an inductor or a capacitor depending on the input impedance (Z_{sim}) of the non-resonant antenna structure. The left-hand side negative inductor can be absorbed into L_1. Thus, the final matching network will have in total four components. Explicit equations for optimum circuit parameters of the matching network are given in [P2]. Design rules are also given for the case the inverter-transformer is realized with capacitors.

In derivation of the equations for the optimum values of C_1 and L_1, it is assumed in [P2] that Resonator 2 behaves like a series-RLC-resonant circuit. Of interest would be to see how this assumption, and thus the design equations of [P2] hold when applied to a realistic coupling element based antenna structure. Fig. 3.3 presents the frequency responses of reflection coefficients obtained when a matching network generated for a realistic antenna structure (see details from [P2]) is connected either to the simulated antenna structure, or to the series-RLC equivalent circuit of the simulated antenna structure. When the equivalent circuit is used as a load, the size of the dual-resonant circle on the Smith-chart equals with that of the circle representing the minimum allowed return loss ($L_{retn} \geq 6$ dB). The same condition for optimum dual-resonant response has been obtained e.g. in [41],[77]. When the simulated antenna structure is used as a load, the dual-resonance circle is slightly moved clockwise along the 50 Ω constant-resistance circle. This can be compensated e.g. by slightly decreasing the value of C_1. Nevertheless, the frequency response is very close to optimum. In [P2], furthermore, almost perfect agreement between the two curves was obtained with 1.8 GHz matching center frequency. The design equations presented in [P2] thus seem to be feasible for use with realistic coupling element based antenna structures. The theoretical relative bandwidth of a single-resonant antenna tuned optimally into dual-resonance with one lossless matching resonator can be expressed as [74]-[77].

$$B_{dr,opt} = \frac{\sqrt{S^2 - 1}}{Q_0}. \tag{3.2}$$

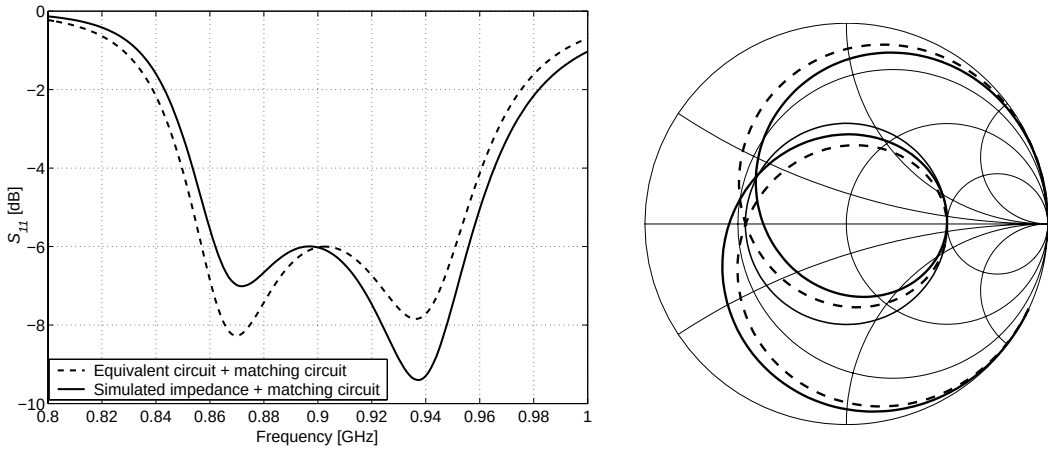

Figure 3.3. *Frequency responses of reflection coefficient obtained when the designed matching circuitry is connected either to the simulated antenna structure (solid line), or to the equivalent circuit of the simulated antenna structure (dashed line). The center frequency of impedance matching is 0.9 GHz. The solid circle on the center of the Smith chart represent* L_{retn} *= 6 dB [P2].*

One should finally note that the component values given by the design equations might not always be exactly realizable with commercially available discrete components. High-Q discrete components falling very close to the optimum values, however, are usually readily available from the market. Moreover, practical realization of a matching network always requires tuning and a few iteration rounds. Theoretical optimum component values provide an antenna designer a good point from which to start the matching network design process.

3.4 PERFORMANCE COMPARISON WITH PIFAS

In order to study the feasibility of the idea of coupling elements, in total four prototypes were designed and thoroughly studied in [P1]. The prototypes were based on two different coupling elements, hereinafter referred as antenna model 1 and antenna model 2. Tuning and optimization of the coupling elements were based on the results obtained with the probe-simulations (see Section 3.2 of this thesis). Two prototypes were manufactured from each antenna model, one for the E-GSM900 band and one for the GSM1800 band. The matching circuitries were implemented as simple tapped microstrip lines. Fig. 3.4 shows the structures of antenna model 1 and antenna model 2.

Antenna model 1:

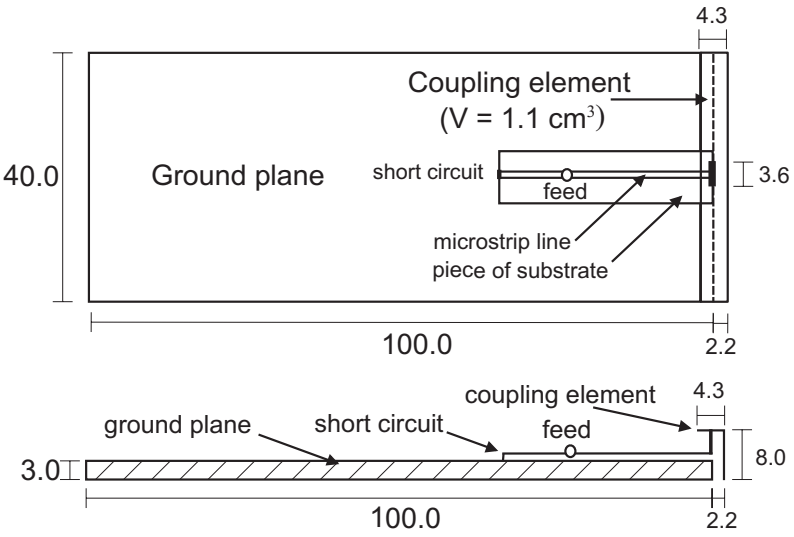

(a)

Antenna model 2:

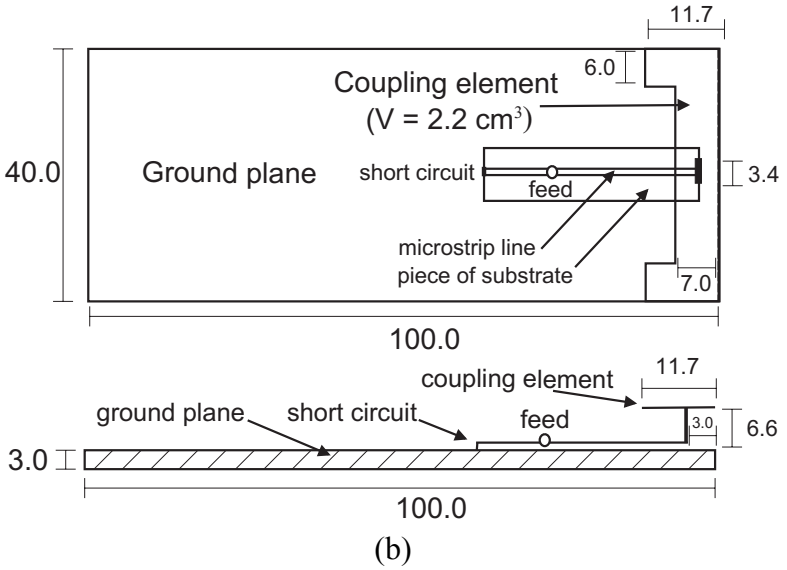

(b)

Figure 3.4. *The structures of (a) antenna model 1 and (b) antenna model 2 with general microstrip line matching circuitries. All dimensions are given in millimeters [P1].*

The coupling element of antenna model 1 occupies a very low volume, only 1.1 cm^3. In order to optimally capture the strong electric fields originating from the end of the chassis, the coupling element has been moved partly outside the top perimeter of the chassis and bent over the end of the chassis. The coupling element of antenna model 2, occupying the volume of 2.2 cm^3, is placed in a more traditional way totally on top of the chassis. To optimize coupling to the wavemodes of the chassis, the shape of the coupling element has been chosen to roughly follow the contour lines shown in Fig. 3.1 (c).

For an antenna designer, it would be useful to know the implications of using optimally shaped coupling elements instead of traditional self-resonant antenna elements on bandwidth, radiation efficiency, and SAR. For reference, two antenna structures with traditionally shaped single-resonant PIFAs (from [37]) as the antenna elements were studied in [P1]. The reference antennas have been designed for the E-GSM900 and GSM1800 systems, and occupy the volumes of 5.4 cm^3 and 2.9 cm^3, respectively. The antenna elements are placed in a traditional way at the height of 6.45 mm fully on top of the chassis (see [37] for complete dimensions). Their resonant frequencies fall very close to those of the prototype antennas studied in [P1].

In [P1], the performance of the coupling element and PIFA based antenna structures were thoroughly evaluated and compared both in free space and in a realistic talk position beside head and hand models. The main findings related to the bandwidths, bandwidth-to-volume ratios, SARs, and radiation efficiencies of the studied antenna structures are summarized in the following sections.

3.4.1 Bandwidth and bandwidth-to-volume ratio

As known from [35], the bandwidth of the combination of an antenna element and chassis is affected by the unloaded quality factors of the antenna and the chassis, the level of coupling between the resonant wavemodes of the antenna and the chassis, and the ratio of the resonant frequencies of the antenna element and the chassis. In the study conducted in [P1], the unloaded quality factor of the chassis and the ratio of the resonant frequencies were fixed. If the unloaded quality factor of the antenna mode is increased, e.g. the antenna element is made smaller in size, a stronger coupling to the wavemode of the chassis is needed to reach the original bandwidth [35]. By applying this argumentation with the results of [P1], it can be claimed that the studied coupling elements excite the dominant wavemode of the chassis more strongly than the reference PIFAs. The volume of antenna model 1, for example, is nearly five times lower than that of the E-GSM900 reference PIFA. Despite this, the bandwidth of antenna model 1 at 900 MHz was clearly higher than that of the reference antenna [P1]. To reach its bandwidth, the coupling element of antenna model 1 needs to couple much more strongly to the wavemodes of the chassis than the reference PIFA. The same logic works also when applied with the bandwidth results obtained at the GSM1800 band [P1].

The so-called bandwidth-to-volume ratio, i.e. the ratio of the relative bandwidth of an antenna structure to the volume of the antenna or coupling element, gives a useful tool for the comparison of antenna structures having different bandwidths and different antenna/coupling element volumes. At the E-GSM900 band, the bandwidth-to-volume ratio of antenna model 1 was over three times larger than that of antenna model 2. The bandwidth-to-volume ratio of antenna model 2, furthermore, was nearly two times larger than that of the reference antenna

[P1]. Similar trend was observed at the GSM1800 band. The strongest and most efficient coupling to chassis wavemode was thus obtained with antenna model 1. Antenna model 2 also utilizes its volume efficiently, but does not represent an optimum arrangement. The weakest coupling to chassis wavemode within the used volume was obtained with the reference PIFAs.

3.4.2 Specific Absorption Rate (SAR)

In [P1], a commercial finite-difference time-domain (FDTD) based electromagnetic solver, SEMCAD (by Schmidt & Partner Engineering AG), was used to investigate the SAR values and radiation efficiencies of the studied antenna structures in talk position. In one simulation setup, the studied antenna structures were placed beside the left ear of a homogenous Specific Anthropomorphic Mannequin (SAM) head model in the standard "cheek" position [17]. In a second simulation setup, also a model of the user's hand [37] holding the phone was included. The minimum distance between the surface of the chassis and the head model was 7 mm.

As a general remark, all studied antenna structures fulfilled the 10 g averaged SAR limits. At both 900 MHz and 1800 MHz, antenna model 1 had clearly the largest SAR values. The SAR values of antenna model 2 were slightly larger than those of the reference antenna. Similar general behavior between the studied antenna structures was obtained both with and without the hand model. The trend apparently resembles the one observed earlier in the bandwidth-to-volume comparison. When coupling to the dominant wavemode of a chassis is increased, e.g. by means of optimum shaping and placement of the exciting element, the amplitude of the chassis wavemodes increases. This increases the amplitude of the antenna structure's near fields, which results in an increase of SAR.

At 900 MHz, the SAR maxima were for all antenna structures located near the middle part of the chassis, as expected [20]. At 1800 MHz, an additional local *SAR* maximum appeared under the coupling element of antenna model 1. The *SAR* maximum of the GSM1800 reference antenna appeared under the antenna element.

3.4.3 Radiation efficiency

Free space:

In free space, the simulated (IE3D) radiation efficiencies of all studied antenna structures were larger than 95 % over the frequency bands of the E-GSM900 and GSM1800 systems [P1]. The result is expected, as the conductivities of the metal parts of the studied antenna structures were equal in the simulations. Moreover, ohmic losses of the used microstrip line matching circuitries are in practice negligible [P1].

Talk position:

Radiation efficiencies at 900 MHz and 1800 MHz, both with and without the hand, followed the same general trend as observed with the SAR results. Antenna model 1 had generally the lowest radiation efficiencies. The radiation efficiencies of antenna model 2 were slightly lower than those of the reference antennas. The lower radiation efficiencies of antenna model 1 can be partly explained by its stronger excitation of the chassis wavemodes. It can be also

expected that electric field components tangential to the surface of the head model are fairly strong under the coupling element of antenna model 1. This most likely leads to an additional power loss in the user's head compared to more traditional designs, such as antenna model 2 and the reference antennas, in which the exciting element is placed fully on top of the chassis.

The above-described results are fully supported by the observations of [37], i.e. that there exists a clear connection between the bandwidths, radiation efficiencies in talk position, and SARs of mobile terminal antennas. When bandwidth (or bandwidth-to-volume ratio) is increased by a stronger coupling to the chassis wavemodes, SAR increases and radiation efficiency in talk position decreases. Decreasing of SAR (and increasing of efficiency) without severely affecting the bandwidth could be attempted by changing the current distribution of the chassis, as described in [59],[78]. Nevertheless, the above-described trade-off obviously needs to be accepted when coupling elements are used instead of self-resonant antenna technologies, such as PIFAs. The improvement obtained in bandwidth-to-volume ratio with coupling elements, however, is multifold compared to the respective increase of SAR and decrease of radiation efficiency in talk position [P1]. Thus, coupling elements offer a competitive and promising alternative for traditional antenna technologies.

4 Multi-band and multi-resonant antenna structures

4.1 INTRODUCTION

The number of radio systems in which modern mobile terminals are required to operate is growing steadily. In addition to the European E-GSM900 (880 MHz – 960 MHz) and GSM1800 (1710 MHz – 1880 MHz) systems, many new mobile terminals are also able to operate in the GSM850 (824 MHz - 894 MHz) and GSM1900 (1850 MHz – 1990 MHz) systems. These quad-band terminals are often equipped with support for Universal Mobile Telecommunication System (UMTS), which operates at the frequency range of 1920 MHz – 2170 MHz. In addition to the above, many modern mobile terminals directed for business users are able to operate according different Wireless Local Area Network (WLAN) standards. Currently WLAN systems work at the ISM band (2400 MHz – 2500 MHz) and at the 5 GHz region (5150 MHz – 5825 MHz). In addition to WLAN, there exist many non-cellular systems that are already in use or are planned to be incorporated in mobile terminals. These include e.g. Bluetooth (ISM band), Global Positioning System (GPS), FM radio, Ultra Wideband (UWB) systems and Radio Frequency Identification (RFID). A great deal of expectations has been put into the Digital Video Broadcasting for Handheld (DVB-H) system (470 MHz – 860 MHz), which has lately been taken into commercial use in Europe.

While new radio systems have been actively taken into commercial use, the trend in the market has been towards shorter and significantly thinner terminal devices with very limited space available for internal antenna elements. Novel low-volume and low-profile antenna technologies are thus urgently needed. In the following, first traditional ways of implementing internal multi-band and multi-resonant antenna structures are briefly reviewed[1]. This is followed by discussion on the implementation techniques of coupling element based multi-band and multi-resonant antennas, including the contributions of this thesis [P2],[P3],[P4],[79],[80].

4.2 TRADITIONAL INTERNAL ANTENNA SOLUTIONS

4.2.1 General

Different variants of PIFAs, IFAs, and planar monopoles are the most common internal antenna solutions used in mobile terminals. The antenna elements are usually self-resonant, i.e. impedance matching takes place inside their metallic structure. The resonant frequency is adjusted by tuning the electrical length of the current path provided by the antenna element to match quarter-wavelength at the desired operating frequency. Below 1 GHz, like at the E-GSM900 band, the physical length of the current path becomes so large that some kind of meandering of the antenna element is usually needed to keep its dimensions compact. After all the necessary resonances have been excited, the feed of the antenna element must be appropriately coupled with the resonances. This is usually done by tuning the location of the feed and possibly also some dimensions of the antenna element. Finally, in order to maximize the bandwidth-to-volume ratio of the antenna structure, the shape and location of the antenna

[1] In this thesis, the term "multi-band" is used to refer to an antenna that uses two or more resonances to cover two or more clearly separate frequency bands, e.g. those of the E-GSM900 and GSM1800 systems. The term "multi-resonant" is used to refer to an antenna that has two or more closely-tuned resonances within an individual band of operation, e.g. that of the E-GSM900 system.

element should be selected so that it couples as strongly as possible to the wavemodes of the chassis. This aspect has often not been considered in papers where different types of self-resonant multi-band antenna structures have been reported for mobile terminals.

4.2.2 The general principle of multi-band antennas

A well-known way to create two separated resonances with a single-feed antenna element is to shape the element in such a way that it provides two quarter-wavelength current paths with different resonant frequencies. The principle was for the first time applied in [60] in the implementation of a dual-band GSM900/GSM1800 PIFA, and later in numerous other publications like in [9],[34],[61],[62]. The idea has also been widely used with planar monopole antennas [81],[82] and IFAs [83], to give only a few examples.

4.2.3 Multi-band antennas with multiple resonances per band

As shown in [77],[84], the bandwidth of a single-resonant shorted patch can be more than doubled by dividing the patch into two narrower shorted patches, of which only one is actively fed while the other one works as a parasitic element. Parasitic radiating elements have been widely used for adding one or more resonances to the lower [85],[86] and upper [9],[34],[62],[86] bands of dual-band PIFAs. The idea has also been applied to increase the impedance bandwidths of dual-band planar monopole antennas [82],[87].

One way to simultaneously obtain a multi-resonant response in both the lower and upper bands of a basic dual-band GSM antenna is to add a lumped element matching network to the feed of the antenna element [73],[88]. The lower band of a dual-band antenna can also be made dual-resonant by connecting a distributed high-Q matching resonator appropriately to the antenna element [89]. Obviously, the same technique can be used at the upper band.

Another technique to obtain (effectively) a multi-resonant response within individual bands of a multi-band antenna is to apply electrical frequency tuning within those bands. Examples are given e.g. in [83],[90]. Frequency tunable antennas have the disadvantages of some extra losses caused by the tuning circuit and distortion caused by non-linear tuning components.

4.3 COUPLING ELEMENT BASED ANTENNA SOLUTIONS

4.3.1 General

There exist a few general principles of implementing multi-resonant and multi-band antenna structures for mobile terminals by using the idea of coupling elements. As described in [51], one or more matching circuitries can be connected to a single non-resonant coupling element. The matching center frequencies associated with each matching circuitry can be tuned close to each other (multi-resonant response), or clearly apart from each other (multi-band response). The connection between the matching circuitries and the coupling element can be arranged by two means. One way is to simultaneously connect all the matching circuitries to the coupling element. If isolation between the feeds of the matching circuitries gets too low, it can be feasible to arrange the connection with an RF switch.

Another general principle, as described in [51], is to connect a single matching circuitry to one or more coupling elements. Each coupling element can be assigned its own frequency band, e.g. that of the E-GSM900 or GSM1800 system, after which the coupling elements can be individually optimized according to the specific needs of their operating bands. The matching circuitry is designed such that it provides impedance matching at the desired frequency bands. In practice, a feasible solution can be to use several matching circuitries connected to several coupling elements.

4.3.2 Patch-type coupling elements

Single-resonant antenna structures based on traditional patch-type (capacitive) coupling elements have been demonstrated at cellular frequencies in [35],[51]-[54],[91],[P1]. The next step is to tune the combination of a chassis and non-resonant coupling element into dual resonance. Explicit design equations for a matching network, which can be used for tuning coupling element based antenna structure optimally into dual resonance with a minimum circuit complexity have been derived in this work [P2] (see Section 3.3.4). Dual-resonant matching of coupling elements has been demonstrated in practice in this work [79],[80],[P3], and in [55],[91]-[93].

A coupling element based quad-band antenna structure being able to cover the frequency bands of the GSM850, E-GSM900, GSM1800 and GSM1900 systems with at least 6 dB return loss and high radiation efficiency ($\geq$ 75% in free space) was introduced in this work [79],[80],[P3]. According to the author's knowledge, it is the first published coupling element based antenna structure capable of such performance. Fig. 4.1 (a) presents the layout of the antenna structure. The antenna structure has two optimally shaped and located coupling elements, one for the lower GSM bands and one for the higher GSM bands. The coupling elements have a very low profile (4 mm) and they occupy a total volume of only 0.7 cm^3. Both coupling elements have their own matching circuits (see Fig. 4.1 (b)), which are used to produce dual-resonant matching for both the lower and upper GSM bands. At the end of the matching arrangement, the feeds of the lower- and upper-band matching circuits are connected together to get just a single feed for the whole antenna structure. The simulated 10 g averaged SAR values of the antenna structure fulfill the specifications (Table 2.1).

Following this work [79],[80],[P3], a quad-band GSM antenna structure incorporating two optimally placed coupling elements was demonstrated in [92]. The coupling arrangement occupied a total volume of 3 cm^3 and had the height of 10 mm (5 mm on both sides of the chassis). Both coupling elements had their own matching circuits implemented as simple tapped microstrip lines. A novel balun-type resonant screen (see details from [92]) was used to make the chassis (100 mm x 40 mm) of the terminal appear as a $\lambda/2$-resonator at 1.8 GHz, and thus make the upper band of the antenna structure dual-resonant. A similar technique was used later in [94] to increase the upper band performance of multi-band PIFAs. In [92], the resonant screen simultaneously worked as a capacitive load for the chassis, thus increasing its electrical length and improving bandwidth at the problematic GSM850/E-GSM900 bands.

Frequency tunable matching circuits

It was demonstrated in [91] by simulations that it is possible to cover the E-GSM900, GSM1800 and UMTS system bands with a frequency tunable matching circuitry connected to

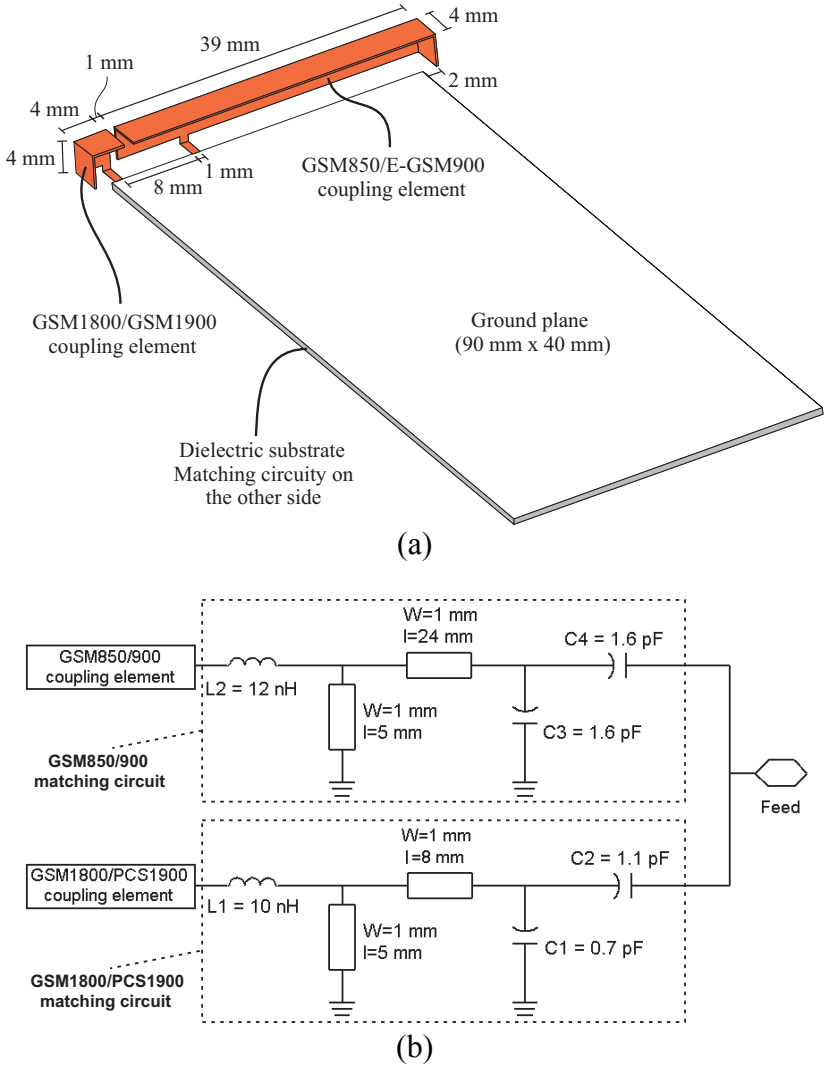

Figure 4.1. *(a) Geometries of the coupling elements and the chassis of the quad-band antenna structure reported in [P3], and (b) a schematic of the matching circuitry. The blocks on the matching circuitry represent microstrip lines (W = width and l = length).*

a simple coupling element. A Single-Pole Five-Throw (SP5T) switch connected to the feed of the coupling element was used for selecting one of five matching circuitries, each having different matching center frequencies and its own feed. A similar idea was applied at the DVB-H band in [93],[95]. The matching circuitry had two SP2T switches, one at the feed of the coupling element and one at the feed of the matching circuitry. It was demonstrated that it is possible to meet the realized gain specifications of the DVB-H system [96] with a low-profile coupling element having the volume of only 1.5 cm^3.

As well-known, the power loss caused by a resistive component, such as an RF switch, is directly proportional to the square of the current flowing through the component. Thus, in order to minimize power loss in a frequency tunable matching circuitry, switches should be placed in high-impedance, i.e. low-current locations. As known e.g. from [P2] and [P4], the input impedance of a patch-type coupling element is usually fairly low at cellular frequencies. In power loss point of view, the input of a coupling element therefore does not represent an

optimum location for a switch. As part of this thesis, a novel frequency tunable dual-resonant matching circuitry optimized with respect to power loss was designed for coupling element based antenna structures. The first, simulation-level study of matching circuit was reported in [P4]. A schematic of the matching circuit is shown in Fig. 4.2 (a).

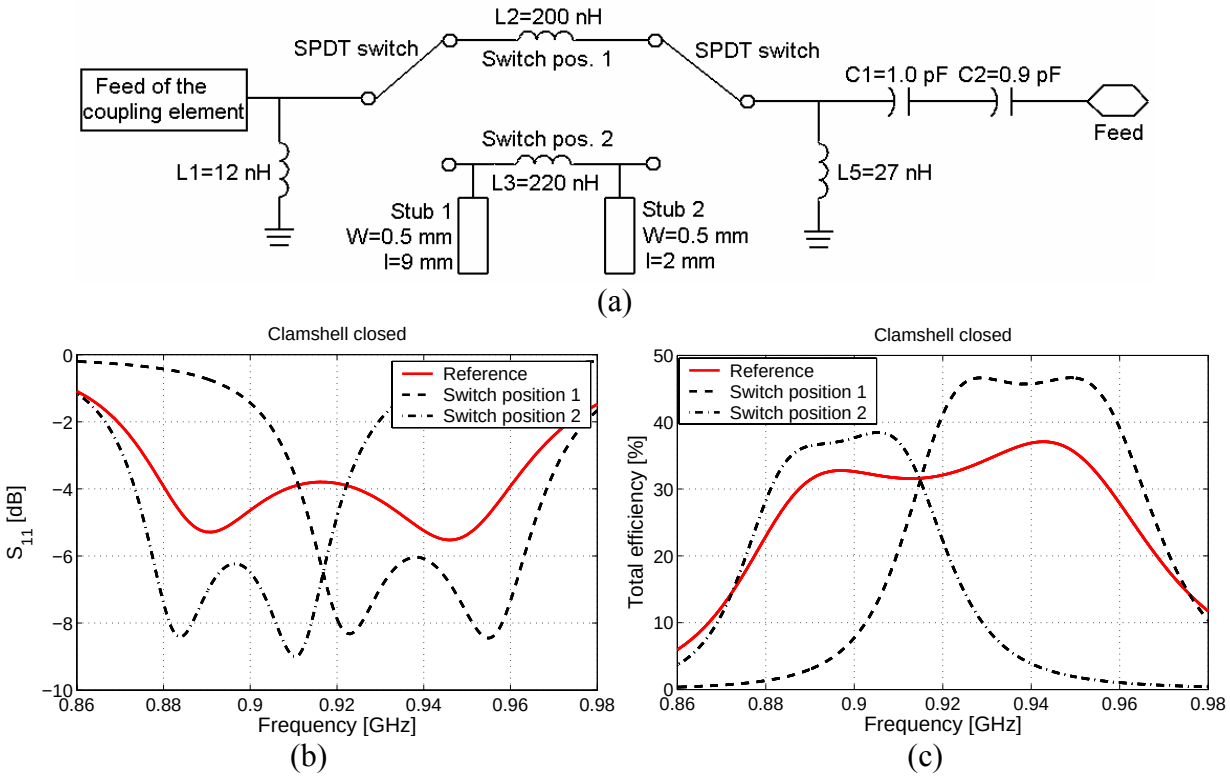

Figure 4.2, *(a) A schematic of the frequency tunable matching circuitry introduced in [P4]. Stub 1 and Stub 2 represent open-circuited microstrip lines (W = width and l = length). (b) The simulated frequency responses of reflection coefficient, and (c) the simulated total efficiencies obtained with the frequency tunable and reference matching circuitries.*

Inductor L1 in Fig. 4.2 (a) controls the resonant frequency of the antenna structure when the switches are in the up-position (Switch pos. 1). Resonant frequency can be tuned down with a parallel, open-circuited microstrip line (Stub 1) placed after the first switch (in Switch pos. 2). Stub 1 can be alternatively implemented as a parallel shorted inductor. When the resonant frequency of the antenna structure is tuned, both the size and location of the dual resonance circle on the Smith-chart become detuned. The detuning can be compensated by tuning the second component of the matching circuitry (L3), and by adding another stub (Stub 2) before the second switch. The topology of the matching circuitry has been chosen such that both switches are in a high-impedance, i.e. low-loss location. In [P4], the matching circuit was applied in switching between the up- and down-link bands of the E-GSM900 system. With the frequency tunable matching circuitry, clearly better matching and larger total efficiency is obtained over the E-GSM900 band than with the passive reference matching circuitry[2]. The next step would be to design and build a prototype, and measure it. The distortion caused by

[2] The topology of the passive reference matching circuitry is similar to the one of the GSM850/900 matching circuitry shown in Fig. 4.1 (b). Impedance matching with the reference matching circuitry has been optimized according to L_{retn} = 4 dB criterion, which gives the best available matching over the E-GSM900 band.

the non-linear switches should be studied with two-tone intermodulation distortion measurements. The results of [97] indicate that there might be a trade-off between the distortion and the power loss caused by a non-linear tuning component [41].

4.3.3 Loop-type coupling elements

One way to excite the wavemodes of the chassis is to use loop-type (inductive) coupling elements placed in the locations of magnetic field maxima of the wavemodes [51]. The first and so far the only multi-band application of the idea, according to the author's knowledge, was reported in [56]. Two low-volume loop-type couplers, one for the GSM850/E-GSM900 bands (V = 0.11 cm^3) and one for the GSM1800/GSM1900/UMTS bands (V = 0.08 cm^3), were placed on top of a 5 mm narrow strip interconnecting the base and flip parts of a clamshell phone in the open position. Each coupler had an integrated matching circuit realized as a simple capacitive termination. The lower bands were covered with larger than 8 dB return loss and the higher bands with larger than 10 dB return loss. It was also demonstrated in [56] that it is possible to cover the DVB-H band with larger than 7 dB return loss by an inductive coupling element and a capacitor both integrated within the hinge of a clamshell phone.

4.3.4 Coupling via a slot on a chassis

Excitation of chassis wavemodes can also be arranged with a feed placed over an impedance discontinuity on a chassis, such as a slot. It was demonstrated in [57] that it is possible to obtain better than 6 dB matching from roughly 0.9 GHz to roughly 3.7 GHz by placing direct feeds over the two slots of an E-shaped chassis having the dimensions of 105 mm x 65 mm. The wide-band operation was possible due to very strong excitation of several resonant wavemodes of the chassis and the $\lambda/4$ resonances of the slots.

It was shown in [58] that it is possible to meet the realized gain specifications of the DVB-H system with 4 dB margin by placing a direct feed over one of the two slots of a meandered, S-shaped chassis having the dimensions of 130 mm x 75 mm. A simple, L-section matching circuitry connected to the direct feed was used to tune the antenna structure into dual resonance with larger than 1.6 dB return loss over the DVB-H band.

In [98], a slot placed in the middle of a 100 mm x 40 mm chassis was fed by an open-ended microstrip line oriented in parallel with the slot (crossing the slot at one point). A triple-resonant response was obtained with contributions from the lowest order resonant wavemode of the chassis, $\lambda/4$ resonance of the slot, and the open-ended stub of the microstrip line. The antenna structure was able to cover the frequency range of 0.9 GHz to 2.7 GHz with larger than 6 dB return loss and larger than 70 % total efficiency.

The results of [57],[58],[98] demonstrate that placing a feed over a slot on a chassis provides a volume-efficient way of realizing broad-band antenna structures for mobile terminals. It can be suspected, however, that the volume both above and under the slot needs to be kept free of any metallic objects, such as the display and battery of a terminal, and possible EMC-shields usually existing inside modern mobile terminals. Furthermore, it can be suspected that the effect of the user's head and hand on the performance (efficiency and matching) of a slot-based antenna structure can be larger than on the performance of a traditional antenna structure having a solid chassis. These aspects have not been considered in [57],[58],[98].

5 Radiation characteristics of mobile terminal antennas in wide frequency range

5.1 INTRODUCTION

Based on [5],[29]-[40], it is clear that the bandwidth, radiation efficiency in talk position, and SAR of mobile terminal antennas are strongly affected by the resonant wavemodes of the chassis. These studies have been mainly carried out with self-resonant antenna elements at single frequencies, typically at 900 MHz and 1800 MHz, by changing the physical dimensions of the chassis, and thus the resonant frequencies of the wavemodes of the chassis. Another approach, perhaps a more realistic one, is to study the bandwidth, radiation efficiency in talk position, and SAR as a function of frequency while keeping the size of the chassis constant. The idea of coupling elements suits particularly well for this purpose, as the structure of a non-resonant coupling element is not tied to any specific operating frequency. Relative bandwidth, for example, can be studied as a function of frequency (Section 5.2.1) by simply tuning a separate matching circuitry, as demonstrated in [P1],[P4],[P5]. Similarly, radiation efficiency in talk position, and SAR can be studied over wide frequency band by applying the idea of coupling elements [P5] (Section 5.2.2).

In recent years, foldable clamshell-type phones have become very popular, and several antenna solutions for those have been suggested, e.g. [56],[99]-[102]. When a clamshell phone is opened or closed, it is clear that also the characteristics of the resonant wavemodes of the chassis of the phone become affected. For an antenna designer, it would obviously be useful to understand the behavior of the wavemodes of the chassis when the mechanical use position of the phone changes. Furthermore, an antenna designer should make sure that high enough total efficiency is obtained in all relevant mechanical use positions of the phone. In general, these aspects have attained very little attention in scientific contributions reporting antenna structures for clamshell phones. To fill this gap, the radiation properties of the resonant wavemodes of the chassis of a clamshell phone were studied systematically as part of this work [P4] with help of coupling elements (Section 5.3). Also, the effect of opening and closing a clamshell phone on antenna performance was investigated in [P4].

5.2 BANDWIDTH, SAR AND EFFICIENCY OVER WIDE FREQUENCY BAND

5.2.1 Bandwidth

The bandwidth of the combination of a non-resonant coupling element and a chassis can be studied as a function of frequency by simply tuning the matching circuitry. Application of the idea was for the first time demonstrated as part of this work in [P1]. Later, the approach was also used in [P4],[P5], and by other authors in [50]. If bandwidth is studied in a wide frequency band, like in [P1],[P4],[P5],[50], both the topology and the component values of the matching network need to be optimized individually for each matching frequency. In [P1], for example, four different L-section matching circuit topologies were needed to cover the frequency range of 0.5 GHz – 4.1 GHz.

In [P5], the behaviour of the bandwidths, radiation efficiencies in talk position, and SAR values of two antenna models based on coupling elements having the same volumes (2.9 cm^3) and heights (6.6 mm) were studied over the frequency range of 0.6 GHz - 6 GHz by

simulations. The coupling element of antenna model 1 was placed in a traditional way fully on top of the chassis, similarly as in Fig. 3.4 (b). The coupling element of antenna model 2 was located and shaped more optimally (similarly as in Fig. 3.4 (a)) to obtain stronger coupling to the wavemodes of the chassis. Both antenna models were studied in free space and in the standard "cheek" position [17] beside a SAM head model, with two different hand models (from [37]) holding the phone. Hand model 1 models mainly the palm of a hand. Its fingers are very short, and the distance between the palm and the chassis is only 2 mm [37]. In hand model 2, the distance between the palm and the chassis is clearly larger, 49.5 mm [37]. Material parameters for the head and hand models were computed separately for each simulation frequency by using the parametric model reported in [103]. According to the author's knowledge, wideband studies similar to this work [P5] have not been reported before in open literature. Fig. 5.1 presents the 6-dB relative bandwidths obtained when the simulated input impedances of the coupling elements have been critically matched to 50 Ω at each simulation frequency by a lossless lumped element L-section matching circuitry.

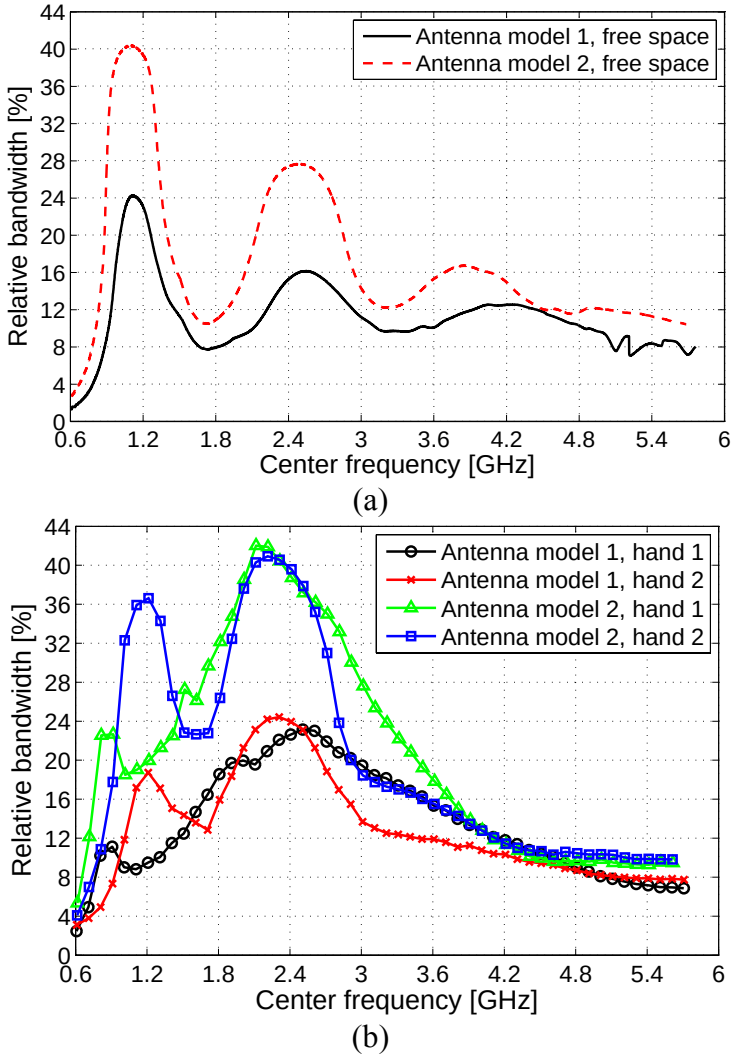

Figure 5.1. *Relative bandwidths ($L_{retn} \geq 6$ dB) as a function of frequency for the two antenna models studied in [P5]. (a) Results obtained in free space, and (b) results obtained with the phone positioned next to a head model (d = 7 mm) and two different hand models.*

Generally higher bandwidths are obtained both in free space and in talk position with antenna model 1, whose coupling element excites the wavemodes of the chassis more strongly than that of the antenna model 2. The strong effect of the resonant wavemodes of the chassis on the relative bandwidth can clearly be seen from the bandwidth curves. In general, the amplitude of chassis wavemodes and thus the impedance bandwidth reaches its maximum when the operating frequency equals with the resonant frequencies of the wavemodes of the chassis [P5]. Similar result has been obtained in studies conducted at single frequency by changing the physical length of the chassis [5],[29]-[37].

In free space, the first three dipole mode resonances of the 100 mm long chassis are located at around 1.2 GHz, 2.5 GHz, and 4 GHz. At the first order resonance, the electrical length of the chassis is roughly $0.4\lambda_0$, which is somewhat less than the effective electrical length of the chassis ($0.5\lambda_0$). The second and third order resonances occur when the electrical length of the chassis corresponds to roughly $0.9\lambda_0$ and $1.4\lambda_0$, respectively. Previous studies [5],[29]-[37] have only considered chassis lengths up to $1.1\lambda_0$, and have thus missed the third resonance and everything above it.

Based on the information available from Fig. 5.1 (b), it was concluded in [P5] that the type of the hand model does not have significant effect on the resonant frequency of the second order resonance of the chassis. Examination of the real parts of the simulated input impedances of the coupling elements[3], however, reveals that the conclusion of [P5] is not correct. With hand model 1, three resonances located at around 850 MHz, 1.8 GHz, and 2.4 GHz can be found from the input impedances (not shown here) of both antenna models. These resonances can be attributed to the first, second, and third order resonances of the chassis, which have been tuned down in frequency by roughly 30%, 33%, and 42% compared to the free space resonant frequencies, respectively. The behavior is expected, as hand model 1 covers a large part of the surface of the chassis with a very short distance. The first and third resonances of the chassis can be observed as clear bandwidth peaks at around 850 MHz and 2.4 GHz. The second resonance of the chassis is clearly visible only with antenna model 1.

With hand model 2, the first and second order resonances of the chassis are located roughly at 1.2 GHz and 2.3 GHz. Apparently, the distance between the palm of hand model 2 and the surface of the chassis is so large that the resonant frequencies of the chassis stay almost unchanged compared to the corresponding free space values. Nevertheless, it is obviously important to take the user's head and hand into account when studying the impedance bandwidths of mobile handset antennas.

Above roughly 3 GHz, the fluctuation of bandwidth starts to settle and the amplitude of the currents flowing on the chassis decreases rapidly [P5]. Also, the bandwidths of antenna model 1 and antenna model 2 approach each other. The contribution of the longitudinal dipole modes of the chassis on radiated power can be thus expected to be fairly weak above 3 GHz. The conclusion is supported by the results of [P1], in which roughly equal bandwidths were obtained at frequencies above 3 GHz with a coupling element situated on top of the shorter end of a chassis and with the same coupling element situated on top of an infinite ground plane.

[3] The real part of the input impedance of a patch-type coupling element has typically local maxima at the resonances of the chassis, which can be seen e.g. from the Smith-chart plots of [P1] and [P4].

5.2.2 SAR and radiation efficiency in talk position

Fig. 5.2 presents the simulated 10g averaged SAR values (in the head model) and radiation efficiencies of the antenna models studied in [P5] as a function of frequency.

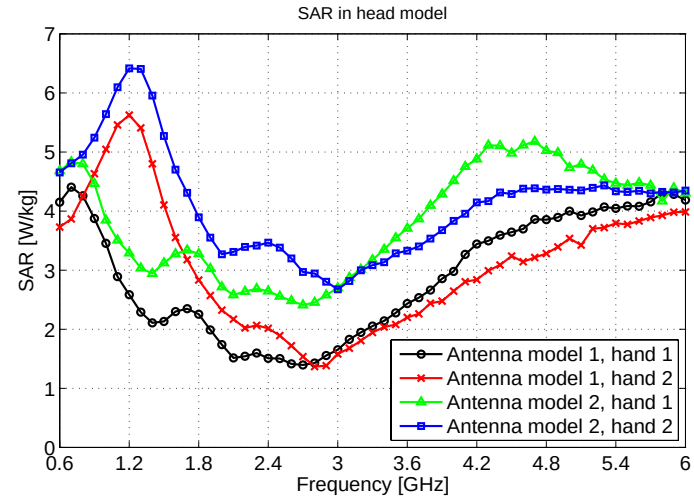

(a)

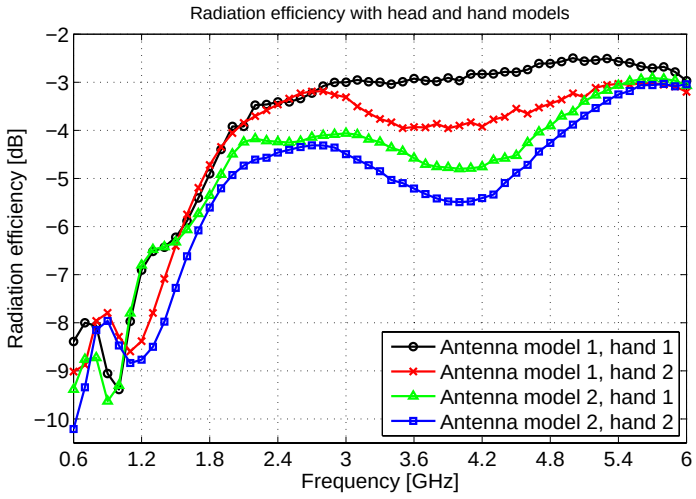

(b)

Figure 5.2. *(a) 10g averaged SAR values in a head model and (b) radiation efficiencies in talk position as a function of frequency for the two antenna models studied in [P5]. Two different hand models have been included in the simulations. Antenna input power has been* P_{in} *= 1 W.*

Two local SAR maxima on the head model were observed in the simulations conducted in [P5], the first one under the middle part of the chassis and the second one under the coupling elements. Below roughly 3 GHz, the first local SAR maximum caused by the wavemodes of the chassis is dominant. When the frequency increases towards 3 GHz, the wavemodes of the chassis become weaker [P5], and thus the 10g averaged SAR has a decreasing trend. Respectively, the wavemodes of the antenna element become stronger as frequency increases. The crossing point in SAR is at about 3 GHz, above which the local SAR maximum under the coupling elements is stronger than the local SAR maximum under the middle part of the chassis [P5]. The change in the location of the global head SAR maximum can be clearly seen

in Fig. 5.2. (a); at around 3 GHz, the head SAR values start increasing strongly, as the wavemodes of the coupling element increase their amplitude.

Below 3 GHz, a similar general trend between impedance bandwidth, radiation efficiency in talk position, and SAR was observed in [P5] as what has been earlier reported in [37],[38]. When bandwidth increases due to a resonance of the chassis, SAR in the head increases and radiation efficiency decreases. This trend is most clearly noticeable near the first order resonance of the chassis. In the whole frequency range, the head SAR values of antenna model 2 are higher and the radiation efficiencies mostly lower than those of antenna model 1. This can be explained similarly as in Sections 3.4.2 and 3.4.3, i.e. by the shapes and locations of the coupling elements. The results of [P5] additionally show that although optimally shaped and located coupling elements are used for exciting strongly the wavemodes of the chassis, the SAR values stay at acceptable level over wide frequency range.

In [P5], 10g averaged SAR values for the hand models were reported as well. With hand model 2, clear SAR peaks located roughly at 1.5 GHz and 3.4 GHz were observed. At around 1.5 GHz, SAR maxima were located in the palm of the hand model, whereas at around 2.4 GHz, the SAR maxima were located in the thumb of the hand model. With hand model 1, clear SAR peaks (maxima at the palm) existed only around 1.6 GHz. No clear connection was found between the resonances of the chassis and the above-described hand SAR peaks. Obviously, a separate in-depth study on the near-fields of the antenna models would be needed to clarify all the details and findings of [P5].

5.3 ANTENNA PERFORMANCE IN CLAMSHELL-TYPE PHONES.

In most contributions where the performance of internal antennas has been studied in clamshell-type phones, e.g. in [99]-[102], attention has not been given for understanding the resonant wavemodes of the chassis, and their effect on the antenna performance. Futhermore, antenna performance evaluation has been usually carried out only in the open position of a clamshell phone.

In [46], the theory of characteristic wavemodes [44],[45] was used to study the radiation properties of the chassis of a clamshell phone. The base part of the phone was modeled by a 70 mm x 40 mm (length x width) metal plate and the flip part as a 50 mm x 40 mm plate. The hinge of the phone, i.e. the connection between the base and flip parts, was modeled by a 15 mm long and 40 mm wide metal plate. Both open and closed positions of the phone were studied. Under plane-wave excitation, two dipole modes resonating along the longitudinal axis of the chassis were identified in the open position, the first one resonating at 982 MHz (Q_r = 3.3) and the second one at 1985 MHz (Q_r = 4.0). In the closed position, three longitudinal modes were identified, the first one resonating at 993 MHz (Q_r = 23.5), the second one at 1957 MHz (Q_r = 1.1), and the third one at 3049 MHz (Q_r = 2.4). The first, i.e. the $\lambda/2$-resonant mode of the chassis, had counter-oriented currents flowing on the base and flip parts of the phone, which explained its high Q_r. Currents of the second and third modes, i.e. the λ- and $3\lambda/2$-resonant modes of the chassis, were mainly co-oriented at the opposing parts of the base and flip parts of the chassis, which explains the low Q_r of these modes.

In this work [P4], the radiation properties of the resonant wavemodes of the chassis of a clamshell phone, and their effect on antenna performance were systematically studied over

wide frequency band with help of coupling elements. Part of the findings have been published by the second author of [P4] already in [104]. In the simulations and measurements conducted in [P4], the clamshell phone was modeled by two metal plates of size 70 mm x 40 mm (length x width), connected to each other with a 6 mm long and 4 mm wide metal strip, i.e. the hinge. The coupling element was a simple rectangular patch placed on top of the other short end of the chassis. In both open and closed positions of the clamshell phone, the first three resonant modes of the chassis were clearly distinguishable from the simulated and measured input impedances of the coupling element. In the closed position, for example, the $\lambda/2$ and $3\lambda/2$ resonances of the chassis were visible as clear resonance circles on the Smith chart. Table 5.1 summarizes the resonant frequencies extracted from the simulated impedances. As can be seen, the resonant frequencies of the chassis modes are generally lower than those reported in [46]. This can be explained by the different lengths of the flip parts of the phone models and by the different dimensions of the hinges used in [46] and [P4].

Table 5.1, *Simulated (IE3D) resonant frequencies of the $\lambda/2$ (f_{r1}), λ (f_{r2}), and $3\lambda/2$ (f_{r3}) resonant modes of the chassis of the prototype antenna studied in [P4].*

	f_{r1} [GHz]	f_{r2} [GHz]	f_{r3} [GHz]
Clamshell open	0.77	1.79	2.35
Clamshell closed	0.79	1.58	2.45

The effect of the resonant modes of the chassis of a clamshell phone on antenna performance was investigated in [P4] by studying bandwidth and radiation efficiency as a function of frequency. Fig. 5.3 presents the relative bandwidths (computed similarly as in Section 5.2.1) obtained with three different widths of the hinge. From the results obtained in the open position of the phone, three clear bandwidth maxima located at around the $\lambda/2$, λ, and $3\lambda/2$ resonances of the chassis can be observed. Also radiation efficiency reaches its local maxima at the resonances of the chassis [P4]. Decreasing of the width of the hinge shifts the first and third bandwidth maxima to lower frequencies, while the second maximum remains almost unchanged. This behavior is expected, as narrowing of the hinge makes the chassis electrically longer. The second peak is not affected much as a current minimum at the full-wave resonance of the chassis is located at the hinge.

In the closed position of the phone, only the full-wave (λ) resonance of the chassis has high bandwidth potential, i.e. low Q_r. The $\lambda/2$ resonance of the chassis is of non-radiating type, which shows up as an inherently narrow bandwidth and a dip in the radiation efficiency (see [P4]). The findings above are fully supported by the theoretical results of [46]. The third, i.e. the $3\lambda/2$ resonance of the chassis, is visible in Fig. 5.3 (b) only as a slight rise in the bandwidth. This contradicts with the results of [46], which predict fairly low Q_r for the resonance. By examining simulated current distributions (not shown here), it can be found that currents at the base and flip parts of the phone are counter-oriented at the $3\lambda/2$ resonance, which explains the result of [P4]. In [46], on the contrary, currents on the base and flip parts of the chassis were mainly co-oriented. The difference can be explained by the different dimensions of the hinges used in [P4] and [46]. The electrical length of the hinge affects the distribution of currents on the base and flip parts of the chassis, and thus the Q_r of the chassis wavemodes.

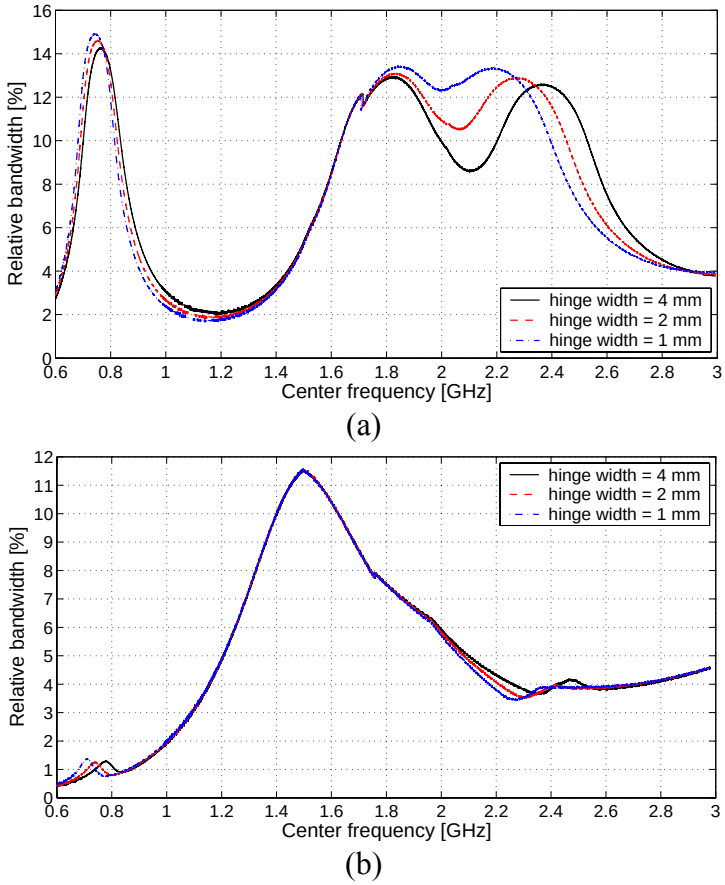

Figure 5.3. *Relative bandwidths obtained in the (a) open and (b) closed positions of the clamshell phone model studied in [P4]. Results are shown for three different hinge widths*

The results of [P4] bring out the problematic nature of designing wideband and high-efficiency GSM850 and E-GSM900 antennas for clamshell phones. In the open position, the half-wavelength resonance of the chassis is located below 800 MHz. Moving of the resonance up in frequency, e.g. by decreasing the electrical length of the hinge, would increase bandwidth potential at the GSM850/E-GSM900 system bands. Closed-position performance, however, would get worse as the non-radiating resonance of the chassis would move to the desired operating band. If the effective electrical length of the hinge is increased, e.g. by making the hinge physically longer or narrower, the half-wavelength resonance of the chassis moves further below 800 MHz, which decreases bandwidth potential in the open position.

In [P4], also the effect of opening and closing the clamshell phone on the impedance matching of the antenna structure was studied at the E-GSM900 band. In case of dual-resonant matching, the size of the resonance circle on the Smith chart decreased significantly when the phone was opened. If the antenna structure was tuned optimally into dual-resonance in the closed position of the phone, very good bandwidth and impedance matching was obtained also in the open position, which can be attributed to the decreased Q_r of the half-wavelength resonant mode of the chassis. It was thus considered advisable to optimize impedance matching for the closed position of the phone. Optimization of impedance matching for the open position of the phone would have resulted in very poor matching in the closed position, as the dual resonant response would have become clearly too over-coupled.

6 Performance evaluation of multi-antenna configurations

6.1 INTRODUCTION

One of the special features of a radio channel is multipath propagation. Due to reflections, diffractions, and scattering from physical objects in the radio channel, transmitted waves arrive at a mobile terminal along multiple propagation paths. In consequence, the incident signal power consists of multiple components, each having its distinctive angle of arrival, phase, and amplitude. At the receiver, the multipath components either add up constructively or cancel each other. When the mobile terminal moves, the relative phases of the multipath components change, which causes rapid variations and deep fades, i.e. fast fading, in the envelope of the received signal power [105].

The so-called Single-Input Multiple-Output (SIMO) systems having a single transmit antenna and multiple receive (diversity) antennas offer a well-known way to mitigate the effects of fast fading [105]-[107]. The benefit of using diversity antenna reception is based on the fact that the signals received by two or more antennas are usually at least partly uncorrelated. If the signal received by one antenna experiences a deep fade, it is likely that at least one of the other diversity antennas provides sufficient signal strength.

Wireless systems with multiple antennas at both ends of the radio link, i.e. Multiple-Input Multiple-Output (MIMO) systems, have been under intensive study during the last decade. In the presence of a rich scattering multipath environment, MIMO systems can provide parallel independent information channels within a given bandwidth, and together with spatial multiplexing (e.g. V-BLAST [108],[109]) offer substantial gains in terms of system capacity [108]-[111]. By applying space-time coding, or its derivatives, MIMO can also be used as a diversity-based scheme to combat the effects of channel fading [112],[113].

At the mobile terminal end of a radio link, the angular power distribution of incident waves is typically non-uniform both in elevation and in azimuth [114],[115],[116]. Moreover, the angular distribution depends strongly on the type of the environment [114]. Thus, when evaluating the true performance of mobile terminal multi-antenna configurations, it is extremely important to study them under realistic channel conditions. A novel test bed for this purpose has been thoroughly evaluated as part of this work in [P6]. Also, it is very important to realistically model the whole metallic structure of the multi-antenna terminal, i.e. the combination of the chassis and the antenna elements. This is due to the significant contribution of the wavemodes of the chassis to the radiation pattern characteristics of mobile terminal antenna structures. For a complete picture on the performance of a multi-antenna configuration, the effect of the user's head and hand should also be considered. In general, there seems to be a shortage of publications where the performance of realistic multi-antenna configurations has been studied empirically in several different types of real, physical environments. To fill this gap, the performance of several realistic mobile terminal multi-antenna configurations has been extensively studied as part of this work in [P7] and [P8].

In this chapter, first the most important performance metrics for multi-antenna terminals and systems are shortly described. After this, a novel multi-antenna test bed [P6] is introduced and its accuracy is discussed. This is followed by a discussion on the main empirical findings reported in [P7] and [P8], but also other studies available in open literature are considered.

6.2 PERFORMANCE METRICS FOR MULTI-ANTENNA TERMINALS AND SYSTEMS

6.2.1 Diversity gain and envelope correlation

Presumably the most common indicator used to describe the diversity performance of multi-antenna terminals in SIMO systems has been diversity gain. It is defined as the difference between the signal-to-noise ratios (SNR) of the signal after diversity combining and the signal of the stronger diversity branch, at a given level of cumulative probability [105]. Usually, diversity gain is computed at the level that 99% or 90% of the signals exceed, i.e. at p = 1% or p = 10% cumulative probability levels, respectively. In theory, diversity gain is maximized if the envelopes of the signals received by the diversity antennas are fully uncorrelated and if all diversity antennas receive the same average power [105]. When envelope correlation or branch power difference increases, diversity gain decreases [105]. This relationship has been demonstrated also experimentally in [117].

6.2.2 Effective Array Gain

Under realistic channel conditions, total efficiency and diversity gain are not adequate performance metrics for describing the power reception properties of mobile terminal multi-antenna configurations [114],[P7]. A more reliable picture is given by the so-called mean effective gain (*MEG*) [116], which has been widely used for describing antenna performance in single-input single-output (SISO) systems. It is defined as the ratio of the mean powers levels received by the studied antenna and a reference antenna in the same physical route [116]. The idea of *MEG* can be also extended to SIMO and MIMO systems, as in [118]. Another approach for characterising the power reception ability of an antenna configuration is provided by the so-called Effective Array Gain (*EAG*) [119]

$$EAG(p) = \gamma_{tot,AUT}(p) - \gamma_{tot,iso}(p), \tag{6.1}$$

where $\gamma_{tot,AUT}$ and $\gamma_{tot,iso}$ are the total powers (SNRs) received by the antenna configuration under test and an isotropic reference antenna at a given level of cumulative probability (p), respectively (see [P8] for illustration). Due to its general definition, *EAG* can be readily used with any number of transmitting and receiving antennas, i.e. both in SIMO and MIMO systems. In order to get a comprehensive insight into the power reception properties of a multi-antenna configuration, it is important to study *EAG* at few different cumulative probabilities, such as at the p = 1% and p = 50% levels [P8].

6.2.3 Capacity and eigenvalue dispersion

The instantaneous theoretical maximum capacity of a MIMO system in which the channel is not known by the transmitter is given by [108]-[111]

$$C^{(i)} = \log_2\left[\det\left(\mathbf{I} + \frac{\rho}{n_t}\mathbf{H}_N^{(i)}\mathbf{H}_N^{(i)H}\right)\right] \quad \text{[bit/s/Hz]}, \tag{6.2}$$

where notation det(•) is determinant, $(\bullet)^H$ is transpose-conjugate, $\mathbf{I}$ is identity matrix, n_t is the number of transmitting antennas, ρ is the average SNR at the receiver, and $\mathbf{H}_N^{(i)}$ is the

normalized channel matrix of the MIMO system for sample number *i*. The elements of the channel matrix $\mathbf{H}_N$, the size of which is n_r x n_t (where n_r is the number of receiving antennas), represent connections between the different transmit and receive antennas. By applying spatial multiplexing under ideal channel conditions[4], one may transmit $\min(n_r,n_t)$ independent data streams simultaneously within a fixed bandwidth [108],[109], which is the fundamental idea of MIMO. In practice, the elements of $\mathbf{H}_N$ are partly correlated, which decreases capacity [120],[121].

In addition to SNR (ρ), the capacity of a MIMO system is affected by the distribution of the eigenvalues of $\mathbf{W}^{(i)} = \mathbf{H}_N^{(i)}\mathbf{H}_N^{(i)H}$. The optimum situation at high SNR region occurs when the eigenvalues, i.e. the gains of the subchannels of the MIMO system, are equal [122]. When the spread between the eigenvalues increases, e.g. due to increased fading correlation, capacity decreases [123]. A useful metric for characterizing the relative spread between the eigenvalues is provided by the so-called eigenvalue dispersion (*EVD*) [124]

$$EVD^{(i)} = \frac{m_g^{(i)}}{m_a^{(i)}} = \frac{\left(\prod_{k=1}^{K}\lambda_k^{(i)}\right)^{1/K}}{\frac{1}{K}\sum_{k=1}^{K}\lambda_k^{(i)}}, \qquad (6.3)$$

which is the ratio of the geometric ($m_g^{(i)}$) and arithmetic means ($m_a^{(i)}$) of the eigenvalues ($\lambda^{(i)}$) of $\mathbf{W}^{(i)}$. Parameter *K* in Eq. 6.3 represents the number of the eigenvalues. Eigenvalue dispersion gets values between $0 \leq EVD \leq 1$, where the maximum value (optimum) represents the case of equal eigenvalues. The logarithmical value (multiplied by *K*) of *EVD* can be understood as the loss in capacity (in bit/s/Hz) from the capacity provided by *K* parallel equal-gain additive white Gaussian noise (AWGN) channels [124].

6.3 MEASUREMENT BASED ANTENNA TEST BED (MEBAT)

6.3.1 General operating principle

The most accurate way of evaluating the performance of a multi-antenna configuration would be to build a prototype, move it along a certain route, and measure the signal power received by it as a function of location. For a complete picture on the performance, the measurement procedure should be repeated in several different types of environments and with several antenna orientations (in talk position etc.). Obviously, the approach becomes easily too time-consuming and expensive. Another option is to measure the directional properties of several radio channels and combine the information with the radiation patterns of the studied multi-antenna configurations. First application of the idea was reported in [115], in which an antenna test bed for Single-Input Multiple-Output (SISO) systems was introduced and used in the evaluation of mobile terminal antennas. In this work [125],[P6], the antenna test bed developed in [115] was extended to cover also SIMO and MIMO systems, and its accuracy was thoroughly evaluated. Hereinafter the test bed will be referred to as measurement based antenna test bed (MEBAT)[5].

[4] i.e. under independent and identically distributed (i.i.d) flat fading Rayleigh channel.
[5] In [P6] the antenna test bed has been called experimental plane-wave based method (EPWBM).

MEBAT relies on radio channel measurements made beforehand. The channels used in this work [P6]-[P8] were selected from the extensive channel library of the Radio Laboratory of Helsinki University of Technology (TKK). The channels have been measured at 2.154 GHz with a real-time wide-band radio channel sounder [126] and a spherical antenna array consisting of 32 dual-polarized microstrip patch antennas [127]. In the measurements, the spherical antenna array and the channel sounder have been located on a motorized trolley, which has been moved along the measurement route at the desired speed. The directional properties of the radio channel have been estimated from the measured channel impulse responses as post-processing using beamforming. Detailed descriptions of the radio channel measurement system and data post-processing are presented in [126],[127].

In MEBAT, the directional data obtained from channel measurements is combined either with the simulated or measured complex 3-D radiation patterns of the studied multi-antenna configuration. Mathematical description of the procedure can be found from [105],[P6]. As an outcome, a vector of complex channel matrices describing the system (SISO, SIMO or MIMO) at each sample, i.e. at each location of the terminal, is obtained. From the channel matrices, all necessary performance metrics can be computed for the antenna configuration and the wireless system under study, such as those discussed in Section 6.2.

Compared to direct measurements, MEBAT saves both time and costs. The performance of a multi-antenna configuration can be evaluated under realistic channel conditions already during the early simulation phase of antenna design process. Furthermore, the radio channel stays exactly the same for all antenna configurations under study, which enables fair comparison between the antenna configurations. If desired, the effect of the user's head and hand can be easily included in the simulated or measured 3-D radiation patterns. The orientation of a terminal can be changed by simply rotating its radiation patterns.

6.3.2 Accuracy evaluation

In [P6], the accuracy of MEBAT was evaluated by comparing the results obtained from direct radio channel measurements carried out with the spherical antenna array to the respective results obtained from MEBAT. Data for the direct measurements was readily available from the channel library of TKK. Several different combinations of environments and the antenna elements of the spherical antenna array were selected for the analysis. At the transmitter side, either single (SIMO) or multiple (MIMO) antenna elements were used. The same environment-antenna combinations were studied with MEBAT based on the measured complex 3-D radiation patterns of the antenna elements of the spherical antenna array.

In the diversity analysis carried out in [P6], 21 different 2 x 1 (n_r x n_t) SIMO systems were considered. Diversity gains were evaluated at p = 10% and p = 50% cumulative probabilities in two ways: as the improvement achieved when the power after maximal ratio combining (MRC) was compared at first to the power of the stronger diversity branch, and second, to the power of the weaker diversity branch. When the weaker branch was used as the reference, the average difference in diversity gains between the two methods was roughly 0.88 dB. When the stronger branch was used as a reference, the average difference between the methods was clearly lower, 0.39 dB at 10% level. In [P6], a realistic mobile terminal multi-antenna configuration was also considered. Fig. 6.1 presents a comparison of the results obtained from direct measurements (DM) and from the MEBAT (see [P6] for details).

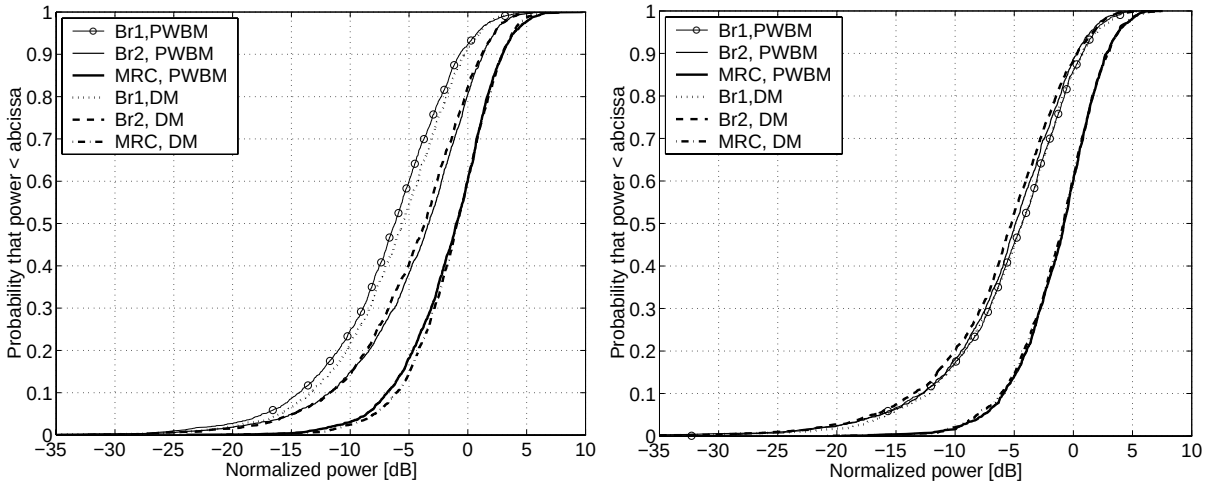

Figure 6.1. *Comparison of the results obtained from direct measurements (DM) and MEBAT (PWBM) in an indoor picocell environment with a realistic mobile terminal multi-antenna configuration placed (a) in free space and (b) beside a human head model [P6]. Br1 and Br2 in the legend denote the two diversity branches of the antenna configuration.*

Based on the results of [P6], it can be claimed that MEBAT provides a rather accurate way of estimating diversity gain in SIMO systems; also in the case of realistic mobile terminal multi-antenna configurations, as indicated by Fig. 6.1. In [P6], the suitability of MEBAT for MIMO system studies was validated by comparing the capacities and eigenvalues obtained from the direct measurements with those obtained from the MEBAT. Several different 2 x 2 and 4 x 4 MIMO systems were considered.

In general, the differences between the two methods were very small, both in terms of mean capacities and mean eigenvalues. The largest reported differences in the mean capacities were 0.56 bit/s/Hz (14% relative difference) and 0.82 bit/s/Hz (10.5%) for the 2 x 2 and 4 x 4 MIMO systems, respectively. In the 2 x 2 MIMO systems, the largest differences in the mean eigenvalues were 0.06 (70%) and 0.19 (17%) from the weakest to the strongest eigenvalue, respectively. In the 4 x 4 MIMO systems, the largest differences in the mean eigenvalues were 0.01 (64%), 0.03 (45%), 0.07 (19%), and 0.29 (17%) from the weakest to the strongest eigenvalue, respectively. Obviously, MEBAT is able to predict fairly accurately the strongest subchannels of a MIMO system, whereas the weakest channels are more problematic.

The discrepancies between the results obtained from direct measurements and from MEBAT can be expected to be mainly caused by the limitations of the channel sounding system, i.e. the combination of the spherical antenna array and the beamforming-based channel estimation algorithm. The system first identifies delay taps from the power delay profile of each snapshot of the channel (usually 5 snapshots/wavelength). The delay resolution of the system is 33 ns, which corresponds to roughly 10 m difference in path lengths [127]. Within each delay tap, there may exist one or more multipath components separated by their directions of arrivals. The channel sounding system enables the separation of these multipath components as long as their angular separation is not less than 40º [127]. More closely spaced waves sum up as complex numbers, which causes uncertainty in the channel estimation. The accuracy of

channel estimation, and thus the accuracy of MEBAT, could be improved by adopting a more sophisticated channel estimation algorithm, such as the SAGE [128].

6.4 EMPIRICAL COMPARISON OF MULTI-ANTENNA CONFIGURATIONS

6.4.1 General

In recent years, many realistic internal multi-antenna configurations have been proposed for mobile terminals, e.g. [129]-[141]. The emphasis in SIMO system studies [129]-[135] has been usually on the evaluation of diversity gain; either directly or by means of envelope correlation and branch power difference. The effect of mutual coupling between the diversity branches of a multi-antenna configuration on total efficiency and envelope correlation has been studied e.g. in [136],[137]. The emphasis in MIMO system studies [138]-[141] conducted with realistic terminal antennas has usually been on the evaluation of capacity (or Bit Error Rate [141]), the correlation properties of the channel matrix, or the radiation efficiency of a multi-antenna configuration. In the papers above, and in many others, proper attention has usually not been paid for the actual power transferring properties, i.e. the effective gains, of the antenna configurations. The *MEG*s of single antenna elements have been considered by some papers [129]-[132],[140], but total effective gains have not been comprehensively studied and related to the other performance metrics. Furthermore, multi-antenna performance has been typically validated experimentally only within one or two different propagation environments.

In this work [P7],[P8], four realistic mobile terminal multi-antenna configurations, each having two internal antenna elements for diversity (see details from [P8]), were comprehensively studied with MEBAT in 12 measured urban, sub-urban and indoor environments. In addition to free space analysis, two of the antenna configurations were further evaluated in talk position beside head and hand models, resulting in total 72 different antenna configuration-environment-combinations. The emphasis in the work was put on experimental and theoretical evaluation of the power transferring properties of the multi-antenna configurations, for which purpose median total received power[6] [P7] and Effective Array Gain (*EAG*) [119],[P8] were used. Also envelope correlation, diversity gain, capacity, and eigenvalue dispersion were considered. According to the author's knowledge, as extensive experimental studies as this work, conducted with realistic phone models and measured environments, have not been reported before in open literature. The main findings of [P7] and [P8] are discussed in the following sections.

6.4.2 Diversity gain and envelope correlation

Diversity gain:

In [P7], the behavior of diversity gain was studied experimentally with realistic mobile terminal antenna configurations. From the results, a clear dependency between diversity gain and envelope correlation was observed. When envelope correlations increased from the range of 0.15-0.32 to 0.49-0.70, diversity gains decreased roughly 1 dB (with low branch power differences). Also the strong effect of branch power difference on diversity gain was clearly

[6] In [P7], the term *MRC MEG* was used to describe the median SNR after maximal ratio combining, but here it is referred simply to as median total received power.

noticeable from the results. When branch power difference increased from roughly 0 dB to roughly 5 dB (envelope correlation 0.15-0.32), diversity gain decreased almost linearly from roughly 6.5 dB to roughly 4.3 dB. The behavior of the results agrees well with [105],[117].

In [P7], it was also considered useful to study the median total powers received by the studied antenna configurations. As an interesting observation, it was noted in [P7] that the antenna configurations which performed the best in terms of median total received power in fact performed the worst in terms of diversity gain. The result was in [P7] logically explained by the strong effect that branch power difference has on diversity gain. In general, an antenna configuration having low branch power difference, and thus high diversity gain, does not necessarily perform well in terms of total received power if its main lobes are badly oriented with respect to the arrival directions of incident waves. The distribution of total received power, or alternatively *EAG*, can be thus considered a more reliable tool than the traditional diversity gain when studying the power transferring properties of multi-antenna terminals under realistic channel conditions.

Envelope correlation:

In [P8], the average (over the studied environments) envelope correlations of the antenna configurations were both in the SIMO and MIMO systems fairly close to each other, and reasonably low. Thus, envelope correlation as a performance metric was not considered to have significant impact on the relative performance between the antenna configurations. One should note, however, that it may be possible to further decrease the envelope correlations by e.g. rearranging the antenna elements with respect to each other and the chassis of the terminal, as indicated by the results of [137]. Of course, the bandwidths of the antenna elements also need to be considered. Strong coupling to the wavemodes of the chassis, and thus higher bandwidths, can be achieved only on top of certain areas of the chassis, which is a limiting factor in antenna positioning. Also the presence of the user's head and hand complicate the design of low-correlation antenna configurations. The head and hand significantly affect the polarization, directivity and orientation of the main lobes of a radiation pattern, which typically leads to increased envelope correlation compared to free space [P8].

6.4.3 Effective Array Gain

Theoretical estimation of *EAG*:

In [P8], the *EAG*s of several antenna configurations were studied both theoretically and experimentally. Fig. 6.2 presents as an example the *EAG*s obtained experimentally with MEBAT in the studied eight SIMO systems. A theoretical estimate for the median (50% cumulative probability) *EAG*s was obtained by modifying the well-known theoretical formula of *MEG* [116] to account for multi-antenna reception:

$$EAG_{50\%} \approx \int \left(\frac{XPR}{1+XPR} \left[G_{1\theta}(\Omega) + G_{2\theta}(\Omega) \right] p_\theta(\Omega) + \frac{1}{1+XPR} \left[G_{1\phi}(\Omega) + G_{2\phi}(\Omega) \right] p_\phi(\Omega) \right) d\Omega \,, \quad (6.4)$$

where $G_{1\theta}$ / $G_{2\theta}$ and $G_{1\phi}$ / $G_{2\phi}$ are the θ- and ϕ-polarized components of the realized gain patterns of diversity branches 1 and 2, *XPR* is cross polarization ratio, and p_θ and p_ϕ are the angular power distribution functions of incident θ- and ϕ-polarized plane waves, respectively.

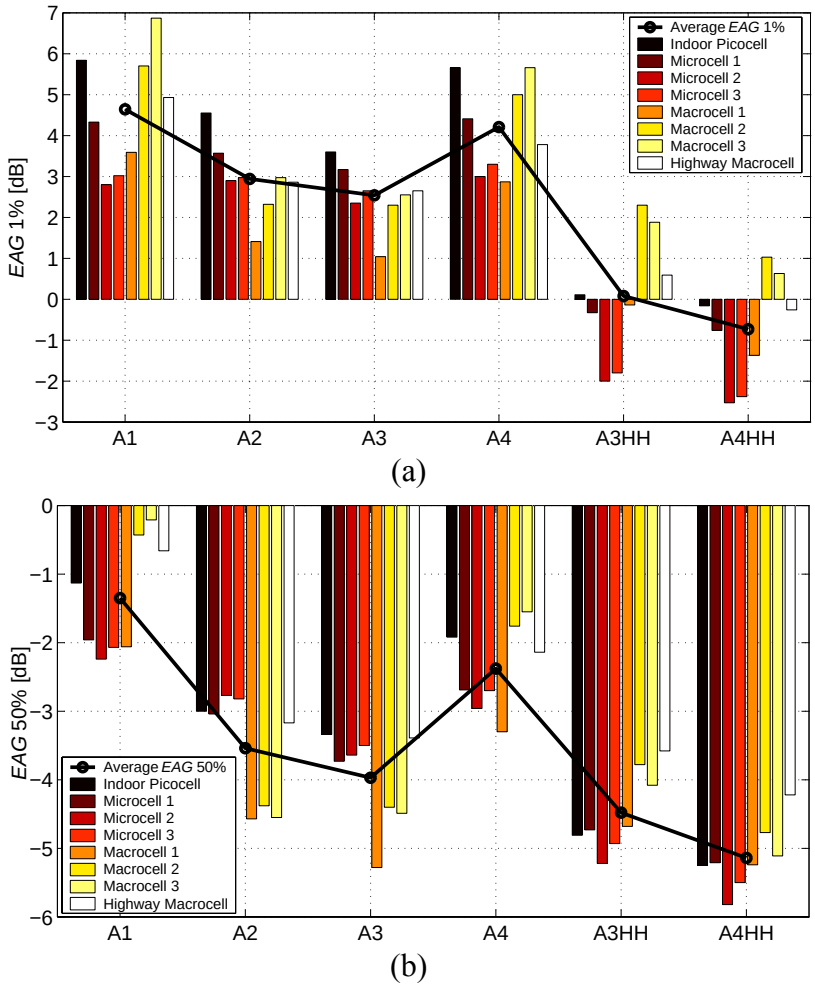

Figure 6.2, *The Effective Array Gains (EAG) of antenna configurations A1-A4 in eight SIMO environments at (a) 1% and (b) 50% (median) cumulative probability levels. Marking "HH" denotes that the user's head and hand have been included in the calculations.*

In [P8], the angular power distribution was assumed uniform in azimuth. Three elevation power distributions were considered: a uniform distribution, a double-exponential distribution [114], and a rectangular distribution [P8]. The uniform distribution assumes that incident power arrives equally from all directions. The double-exponential distribution [114] assumes that most of the indicident power is concentrated on elevation angles slightly above the azimuth plane. The rectangular distribution [P8] assumes that the incident power is equally distributed inside the elevation angle range of $50° \leq \theta \leq 108°$. In the coordinate system, $\theta = 90°$ represents the azimuth plane and $\theta = 0°$ the upper pole of a sphere. The elevation angle range defined above has been obtained from the measurement-based double-exponential distribution [114] by calculating the elevation angle range inside of which 99% of the incident signal power is concentrated. One should note that the use of the rectangular distribution corresponds simply to computing the total power that a multi-antenna configuration radiates within the defined angle range. The contribution of the theta- and phi-polarized components of the antenna configuration's radiation pattern on the radiated power is defined by the *XPR*.

In [P8], the theoretical *EAG*s obtained with the rectangular and double-exponential distributions agreed fairly well with the average (over several environments) median *EAG*s obtained experimentally with MEBAT. The uniform distribution, instead, clearly failed in predicting the experimental results, as expected. It was also shown in [P8] that the *EAG*s estimates obtained with the rectangular distribution ranked the antenna configuration perfectly in the same order as the experimental results; both in the SIMO and MIMO cases. The uniform and double-exponential distributions, on the contrary, failed in predicting correctly the relative ranking. It can be thus concluded that Eq. (6.4) applied with the rectangular distribution provides an accurate and fast way of estimating the average power transferring properties of mobile terminal multi-antenna configurations.

*EAG*s in free space:

In free space, the main lobes of the antenna configurations where mainly vertically polarized and almost omnidirectional in azimuth (see [P8]), obviously due to the strong contribution of the dipole-type wavemodes of the chassis. The largest differences in the average *EAG*s (black circles in Fig. 6.2) were caused by differences in the directions of the main lobes. The lowest average *EAG*s were generally obtained with antenna configurations (A2 and A3), whose main lobes were pointing below the azimuth plane. The highest average *EAG*s were obtained with antenna configurations (A1 and A4), which radiated also above the azimuth plane. The result is logical, as most of the incident signal power is in microcell and macrocell environments typically concentrated on elevation angles above the azimuth plane [114].

In [P8], the isolation between the antenna elements of A2 was fairly low, only 5.3 dB. Therefore, its total efficiency was 0.6 dB to 1 dB lower than those of the other antenna configurations, which had clearly higher isolation (> 12 dB). Such small differences in total efficiencies, however, were found to have no significant effect on the *EAG*s. The result is expected; total efficiency is related to total radiated power, whereas *EAG* accounts for the radiation of an antenna only in the directions from which most of the signal power arrives.

*EAG*s in talk position:

When antenna configurations A3 and A4 were placed in talk position beside head and hand models (below denoted as A3HH and A4HH), their main lobes became very narrow, mainly horizontally polarized, and oriented towards the azimuth plane or slightly above it (see [P8]). Due to the losses caused by the head and hand models, furthermore, the total efficiencies of A3 and A4 decreased significantly (2.6 dB to 5.5 dB) from the free space values.

In the SIMO systems, where vertically polarized transmit antennas were used, the median (50%) *EAG*s obtained in talk position were clearly lower than those obtained in free space (see Fig. 6.2 (b)). The result can be logically explained by the low total efficiencies and wrong (horizontal) polarizations of A3HH and A4HH. In the MIMO systems, where both vertically and horizontally polarized transmit antennas were used, the median (50%) *EAG*s were roughly at the same level both in talk position and in free space. Obviously, A3HH and A4HH benefited from the use of the horizontally polarized transmit antennas.

In addition to the polarizations and orientations of the main lobes, also the widths of the main lobes were in [P8] noticed to have a strong effect on the *EAG* results, especially at the 1%

cumulative probability level. With a very narrow main lobe, as in the case of A3HH and A4HH, the probability of receiving only weak signal becomes high, which degrades *EAG* at low cumulative probability levels (see Fig. 6.2). At 50% cumulative probability, however, an antenna having a narrow pattern can obviously perform very well if its main lobes are well oriented and polarized with respect to the angular power distribution and polarization of incident signals.

Comparison with an ideal isotropic antenna:

By examining the sign and the value of *EAG*, it can be found that how a multi-antenna configuration performs against an ideal isotropic antenna. In the SIMO systems considered in [P8], the average (over the environments) *EAG*s were mainly positive at the 1% cumulative probability and negative at the 50% cumulative probability (see Fig. 6.2). The positive sign at the 1% level is expected, as the studied antenna configurations have the advantage of diversity combining (gain) over the single reference antenna. At 50% level, the reference antenna performed better than the multi-antenna configurations. The result is partly explained by the fact that diversity combining provides the largest benefit at low cumulative probabilities, i.e. against channel fading. In addition, the single isotropic antenna simply radiates more than the multi-antenna configurations (with vertical polarization) to the directions from which most of the signal power typically arrives. This can be seen from the theoretical *EAG*s obtained with the rectangular distribution.

In the MIMO systems considered in [P8], the average *EAG*s were negative at both 1% and 50% cumulative probability levels. Obviously, the isotropic antenna radiating equally with vertical and horizontal polarizations performs very well when dual-polarized transmit antennas are used. The main lobes of the multi-antenna configurations, on the contrary, are not perfectly polarized and oriented with respect to the incident signal power.

An ideal multi-antenna configuration:

Whereas it is very difficult to provide any physical design instructions for a multi-antenna configuration, some general guidelines on optimum antenna characteristics can be derived. First, total efficiency should be maximized, mainly by means of traditional antenna design. The isolation between diversity antennas may be improved e.g. by the method described in [136]. Second, the main lobes of the antenna configuration should be oriented towards the azimuth plane, or slightly above it. The polarizations of the main lobes should be selected according to the polarizations of the transmit antennas. Following the above guidelines should provide high median *EAG* for the multi-antenna configuration. Third, the main lobes of the diversity antennas should cover as effectively as possible the whole azimuth plane without significantly overlapping with each other. Effectively omnidirectional pattern should provide high *EAG* at low cumulative probabilities [P8]. Due to the non-overlapping main lobes, also envelope correlation should be low [141],[142].

One should note that the optimum antenna characteristics most likely cannot be realized in practice. Firstly, the radiation properties of mobile terminal antennas are often significantly affected by the wavemodes of the chassis, which cannot be easily influenced. Furthermore, the optimum antenna characteristics should be obtained in the actual use position of the device. As is well known, the user's head, hand, and other body parts absorb radiation

significantly in certain directions. Also, the exact use position depends largely on the user. Optimum antenna characteristics, however, are worth of pursuing and provide a direction in to which aim.

6.4.4 Capacity and eigenvalue dispersion

Eigenvalue dispersion:

The average (over the studied environments) eigenvalue dispersions obtained in [P8] with the different antenna configurations were all nearly equal, both in free space and in talk-position. A possible explanation for this was found from the nearly equal envelope correlation coefficients. The result suggests that it may be difficult to affect the spatial multiplexing properties of a MIMO system by means of antenna design, at least as far as realistic channel conditions and realistic mobile terminal antennas are considered. In [118], significant differences were found between the eigenvalue dispersions obtained with several different MIMO antenna configurations, but the antennas used were ideal dipoles.

Capacity:

In [P8], a clear dependency was observed between the average *EAG*s and the average capacities of the antenna configurations. At 1% cumulative probability, A1 distinguished from the other antenna configurations with its higher average capacity. Clearly the lowest average capacities were obtained in talk position (A3HH and A4HH). At 50% cumulative probability, A1 again performed clearly the best, whereas the average capacities of the other antenna configurations were closer to each other. Very similar trends were noticeable in [P8] also in the *EAG* results. It was thus concluded that a mobile terminal antenna designer should mainly focus on maximizing the power transferring properties, i.e. the *EAG*, of a multi-antenna configuration. The result is expected, as the eigenvalue dispersions of the antenna configurations were nearly equal.

7 Summary of publications

[P1] Coupling element based mobile terminal antenna structures

This paper presents a comprehensive study on coupling element based mobile terminal antenna structures. The purpose is to increase general understanding on the optimum tuning and design, as well as on the main benefits and drawbacks of coupling elements. Based on MoM simulations, general optimization rules are first derived for capacitive coupling elements. Several optimized prototype antennas are designed and their performance is compared with conventional PIFAs. The results demonstrate that the bandwidth-to-volume ratio of mobile terminal antennas can be significantly improved by using optimized coupling elements instead of self-resonant PIFAs. The results also show that optimization of coupling to the wavemodes of the chassis results in an increased SAR and decreased radiation efficiency in talk position. Finally, a novel way of studying the relative bandwidth of the combination of a coupling element and a chassis as a function of frequency is demonstrated.

[P2] Optimum dual-resonant impedance matching of coupling element based mobile terminal antenna structures

This paper presents a theoretical study on optimum dual-resonant impedance matching of coupling element based antenna structures. Explicit design equations are first derived and given for a matching network, which is optimized for non-resonant antenna structures in terms of circuit complexity. The presented design equations are after this demonstrated to work well when applied with a realistic coupling element based antenna structure. The results indicate that the input impedance of a non-resonant coupling element can be approximated with an adequate accuracy by a series-RLC equivalent circuit.

[P3] A coupling element based quad-band antenna structure for mobile terminals

This paper presents a novel coupling element based quad-band antenna structure for mobile terminals. The antenna structure is able to cover the frequency bands of the GSM850, E-GSM900, GSM1800 and GSM1900 systems with at least 6 dB return loss and high radiation efficiency ($\geq$ 75% in free space). Two optimally shaped and located coupling elements are used, one for the lower GSM bands and one for the higher GSM bands. The coupling elements have a very low profile (4 mm) and they occupy a record-low total volume of only 0.7 cm^3. A single-feed matching circuitry is used to produce dual-resonant matching for the lower and upper bands. The antenna structure meets the European SAR requirements.

[P4] Radiation characteristics of antenna structures in clamshell-type phones in wide frequency range

In this paper, the radiation characteristics of the wavemodes of the chassis of a clamshell phone are studied systematically over wide frequency range (0.6 GHz - 3 GHz) with the help of coupling elements. At first, the resonant frequencies of the first three dipole modes of the chassis are identified from the simulated and measured input impedances of a prototype. After this, the bandwidth potentials of the resonant modes are studied by investigating bandwidth as a function of frequency. The closed position of the clamshell phone is demonstrated to be problematic for an antenna designer, mainly due to the non-radiating type $\lambda/2$-resonance of the chassis, which is located close to the E-GSM900 system band. In order to improve the

performance of the antenna structure in the closed position of the phone, a novel low-loss frequency tunable dual-resonant matching circuitry is proposed and studied by simulations.

[P5] A wideband study of the bandwidth, SAR and radiation efficiency of mobile terminal antenna structures

In this paper, the bandwidth, efficiency in talk position, and SAR of mobile terminal antennas are studied as a function of frequency from 0.6 GHz to 6 GHz. Two coupling element based antenna models are studied by simulations in free space and in talk-position beside a head model and two different hand models. The results confirm that an increase in SAR and decrease in radiation efficiency occur when bandwidth reaches its maximum due to a resonance of the chassis. However, this trend is shown to be invalid above 3 GHz, in which region the wavemodes of the coupling element become dominant. It is also demonstrated that the user's hand can influence significantly the resonant frequencies of the chassis wavemodes.

[P6] Evaluation of the performance of multiantenna terminals using a new approach

In this paper, a novel measurement based antenna test bed (MEBAT) is introduced and its accuracy is thoroughly evaluated. The idea of MEBAT is to combine the complex 3-D radiation patterns of an antenna configuration with a measurement-based estimate of the radio channel. The accuracy of MEBAT is evaluated by comparing the results obtained from it with the results obtained from direct radio channel sounding measurements. It is demonstrated that MEBAT provides an accurate way of estimating diversity gain in SIMO systems, and capacity and eigenvalue dispersion in MIMO systems.

[P7] Advances in diversity performance analysis of mobile terminal antennas

In this paper, the diversity characteristics of several mobile terminal multi-antenna configurations are studied in eight measured environments with MEBAT. The results confirm that diversity gain increases when envelope correlation or branch power difference decreases. The results also show that the traditional diversity gain is not an adequate performance metric for characterizing the power reception properties of multi-antenna configurations in real environments. An antenna configuration performing the worst in terms of diversity gain is demonstrated to perform the best in terms of median total received power.

[P8] Performance analysis and design aspects of mobile terminal multi-antenna configurations

This paper presents a comprehensive analysis of in total 72 different antenna configuration-environment combinations. The motivation is to identify the multi-antenna characteristics that are relevant for the obtained SIMO or MIMO system performance. The emphasis is put on the evaluation of the power reception properties, i.e. the effective array gains (*EAG*), of the multi-antenna configurations. Also total efficiencies, envelope correlations, capacities, and eigenvalue dispersions are considered. The effects various properties of radiation patterns on *EAG* are first identified. It is shown that the median *EAG* of an antenna configuration can be estimated rather accurately by theoretical means. The results indicate that it may be difficult to affect the spatial multiplexing properties of a MIMO system by means of handset antenna design, and that mobile terminal antenna designer should mainly focus on maximizing the *EAG*.

8 Conclusions

The work done in this thesis can be divided into two parts. The first part studies miniaturization and performance enhancement of mobile terminal antennas [P1],[P2],[P3],[P4], and the effect the chassis of a mobile terminal on various important antenna-related parameters [P4],[P5]. The second part of the thesis [P6],[P7],[P8] concentrates on performance evaluation of mobile terminal multi-antenna configurations.

One of the main purposes of this thesis has been to increase general understanding on the main benefits, drawbacks, and application areas of coupling element based mobile terminal antenna structures. The idea behind coupling elements is simple; the coupling element, such as a capacitive patch, is optimized so that it couples as strongly as possible within a certain volume to the dominant wavemodes of the chassis, which maximizes bandwidth. On the contrary to self-resonant antenna elements, impedance matching is done entirely with a separate matching circuitry. The work started with a systematic mapping of those areas of a chassis, which enable strong coupling to the wavemodes of the chassis [P1]. Based on the results, guidelines for the optimum shaping and placement of patch-type coupling elements were given. In order to identify the main benefits and drawbacks of coupling element based antenna structure, several optimized single-resonant prototype antennas were designed, and their performance was compared with that of conventional PIFAs [P1]. The results showed that the improvement in the bandwidth-to-volume ratio of an internal antenna structure can be multifold when optimized coupling elements are used instead of conventional self-resonant PIFAs. The trade-off of increasing coupling to the wavemodes of the chassis, i.e. maximizing the bandwidth-to-volume ratio, was found to be increased SAR and decreased radiation efficiency in talk position. Nevertheless, the SAR values of the prototype antennas fulfilled the European SAR requirements. It was finally concluded that coupling elements offer a competitive alternative for conventional self-resonant antennas.

The next logical step was to extend the scope from single-resonant antenna structures to coupling element based multi-resonant and multi-band antenna structures. Optimum dual-resonant impedance matching of coupling elements was theoretically studied in [P2]. Explicit design equations were derived for a matching network, which can be used for tuning non-resonant series-type RLC loads optimally into dual-resonance with a minimum circuit complexity. The usability of the design equations was tested with a realistic coupling element based antenna structure. The matching networks generated by the presented theory produced nearly optimum dual resonant matching for the studied coupling element. In this work, also a novel coupling element based quad-band antenna structure was reported [P3]. The antenna structure is capable of covering the frequency bands of the GSM850, E-GSM900, GSM1800 and GSM1900 systems with at least 6 dB return loss and high radiation efficiency ($\geq$ 75% in free space). The coupling elements have a very low-profile (4 mm) and they occupy a total volume of only 0.7 cm^3, thus making the structure suitable for the thin terminal devices of the future. According to the author's knowledge, it is the first published coupling element based antenna structure capable of the above-described performance. In this thesis, also a novel frequency tunable dual-resonant matching circuitry optimized with respect to efficiency was designed for coupling elements [P4]. It was demonstrated at the E-GSM900 band by simulations that the proposed matching circuitry provides clearly larger total efficiency than a passive reference matching circuitry. Building of a prototype and measuring of its most important characteristics, including distortion, would be the next steps to proceed with.

The effect of the chassis of a mobile terminal on the bandwidth, efficiency in talk position, and SAR of the antenna structure has been conventionally studied with self-resonant antenna elements at single frequencies by changing the physical dimensions of the chassis. In this thesis [P1],[P4],[P5], the above parameters were investigated as a function of frequency by using coupling elements. The results of a wideband study (0.6 GHz to 6 GHz) [P5] confirmed that an increase in head SAR and a decrease in talk position efficiency occur when bandwidth reaches its maximum due to a resonance of the chassis. This general trend was demonstrated to apply below 3 GHz, in which region the global head SAR maximum was caused by the wavemodes of the chassis. Above 3 GHz, the behavior of the SAR and efficiency were determined by the wavemodes of the coupling element. It was also shown that the user's hand can significantly influence the resonant frequencies of chassis modes, which obviously should be considered when studying the bandwidths of mobile terminal antennas. The results additionally demonstrated that although optimally shaped and located coupling elements are used for exciting the wavemodes of the chassis, the SAR values stay at acceptable level over wide frequency range.

In this thesis [P4], coupling elements were also used to study the radiation properties of the wavemodes of the chassis of a clamshell phone, and the effect of opening and closing a clamshell phone on antenna performance. Both simulated and measured results were presented. The radiation properties of the chassis wavemodes were studied by investigating bandwidth and radiation efficiency as a function of frequency. The half-wavelength resonant mode of the chassis, located somewhat below the E-GSM900 band, was shown to be of non-radiating type in the closed position of the phone. The existence of the non-radiating resonance and also otherwise inherently narrow bandwidth in the closed position were considered to pose a challenge to the implementation of high-efficiency antennas for the E-GSM900 band. The results also suggested that it may be difficult to optimize the performance of an antenna structure simultaneously for the open and closed positions of a clamshell phone by only passive means. Impedance matching, for example, was demonstrated to vary notably as the mechanical use position of the clamshell phone was changed.

The second part of this thesis started with an evaluation work of a novel measurement based antenna test bed (MEBAT) [P6]. The accuracy of MEBAT was studied comprehensively by comparing the results given by it with those obtained from direct radio channel measurements. It was demonstrated that MEBAT provides an accurate way of estimating diversity gain in single-input single-output (SIMO) systems, and capacity and eigenvalue dispersion in multiple-input multiple-output (MIMO) systems. Next, the performance of several mobile terminal multi-antenna configurations were thoroughly investigated in several previously measured environments with MEBAT [P7],[P8]. An extensive set of in total 72 different antenna configuration-environment combinations was considered. The motivation was to identify the characteristics of a multi-antenna configuration that are relevant for the obtained performance. The results confirmed that diversity gain increases when envelope correlation or branch power difference decreases. The results also showed that the traditional diversity gain is not an adequate performance metric for characterizing the power reception properties of multi-antenna configurations under realistic channel conditions. Thus, the so-called effective array gain (*EAG*) was taken into use. Based on a comprehensive analysis of the *EAG* results, guidelines for optimum radiation pattern characteristics were given. It was concluded that the pattern of a multi-antenna configuration should be effectively omnidirectional, which, however, can be difficult to realize in practice due to the influence of

the user's head and hand among others. Also, it was demonstrated that the median *EAG* of an antenna configuration can be estimated rather accurately by theoretical means. The eigenvalue spreads obtained with different antenna configurations in the MIMO systems were nearly equal and capacities were strongly affected by the *EAG*s. The results indicated that it may be difficult to affect the spatial multiplexing properties of a MIMO system by means of handset antenna design, and thus an antenna designer should mainly focus on maximizing the *EAG*.

This thesis provides novel and useful information for the design of mobile terminal antenna structures. It has been demonstrated how the bandwidth-to-volume ratio of the combination of a coupling (or antenna) element and a solid chassis can be maximized by optimizing coupling between the wavemodes of the exciting element and the chassis. The next logical step would be to study how the electrical properties of the chassis can be tuned and controlled in such a manner that the bandwidth-to-volume ratio is further improved. The chassis plays an important role also in case of mobile terminal multi-antenna configurations. The polarizations, directivities and orientations of the main lobes of a multi-antenna configuration are at current cellular frequencies strongly affected by the wavemodes of the chassis. Further work is required to find ways of controlling the wavemodes of the chassis and the antenna element in such a away that optimum radiation pattern characteristics would be approached in the actual use positions of the device.

References

[1] H. A. Wheeler, "Fundamental limitations of small antennas," *Proceedings of the I.R.E.*, vol. 35, pp. 1479-1488, December 1947.

[2] L. J. Chu, "Physical limitations of omni-directional antennas," *Journal of Applied Physics*, vol. 19, pp. 1163-1175, December 1948.

[3] R. F. Harrington, "Effect of antenna size on gain, bandwidth, and efficiency," *Journal of Research of the National Bureau of Standards – D. Radio Propagation*, vol. 64D, no. 1, pp. 1-12, January-February 1960.

[4] H. A. Wheeler, "Small antennas," *IEEE Transaction on Antennas and Propagation*, vol. 23, no. 4, pp. 462-469, July 1975.

[5] T. Taga and K. Tsunekawa, "Performance analysis of a built-in planar inverted F antenna for 800 MHz band portable radio units," *IEEE Journal on Selected Areas in Communications*, Vol. 5, no. 5, pp. 921-929, June 1987.

[6] R. E. Collin, *Foundations for Microwave Engineering*, 2. Edition, New York, 2001, IEEE Press, 924 p.

[7] Y. Suzuki and T. Chiba, "Designing method of microstrip antenna considering the bandwidth," *Transactions of the IECE of Japan*, vol. E 67, no. 9, pp. 488-493, 1984.

[8] H. F. Pues and A. R. Van de Capelle, "An impedance matching technique for increasing the bandwidth of microstrip antennas," *IEEE Transactions on Antennas and Propagation*, vol. 37, no. 11, pp. 1345-1354, 1989.

[9] J. Ollikainen, O. Kivekäs, A. Toropainen, and P. Vainikainen, "Internal dual-band patch antenna for mobile phones," *Proc. AP2000 Millennium Conference on Antennas and Propagation*, Davos, Switzerland, April 2000, CD-ROM SP-444 (ISBN 92-9092-776-3), paper p1111.pdf.

[10] K. R. Boyle, "Mobile phone antenna performance in the presence of people and phantoms," *IEE Technical Seminar Antenna Measurement and SAR (AMS 2002)*, Loughborough University, UK, 2002, 4 p.

[11] K. R. Boyle, "The performance of GSM 900 antennas in the presence of people and phantoms," *Proc. 12th International Conference on Antennas and Propagation (ICAP'03)*, Exeter, UK, March-April 2003, pp. 35-38.

[12] Federal Communications Commission (FCC), Office of Engineering and Technology (OET), *Evaluating Compliance with the FCC Guidelines for Human Exposure to Radiofrequency Electromagnetic Fields, Additional Information for Evaluating Compliance of Mobile and Portable Devices with FCC Limits for Human Exposure to Radiofrequency Emissions*, Supplement C to OET Bulleting 65, June 2001, 57 p.

[13] The Council of the European Union, "Council recommendation on 12 July 1999 on the limitations of exposure of the general public to electromagnetic fields (0 Hz to 300

GHz)," 1999/519/EC, *Official Journal of the European Communities*, L 199, July 1999, pp. 59-70.

[14] ANSI/IEEE Std C95.1, 1999 Edition, *IEEE Standard for Safety Levels with Respect to Human Exposure to Radio Frequency Electromagnetic Fields, 3 kHz to 300 GHz*, New York, USA, April 1999, 73 p.

[15] International Commission on Non-Ionizing Radiation Protection (ICNIRP), "Guidelines for limiting exposure to time-varying electric, magnetic, and electromagnetic fields (up to 300 GHz)," *Health Physics*, vol. 74, no. 4, April 1998, pp. 494-522.

[16] European Std. EN 50360, *Product Standard to Demonstrate the Compliance of Mobile Telephones with the Basic Restrictions Related to Human Exposure to Electromagnetic Fields (300 MHz – 3 GHz)*, CENELEC, Brussels, Belgium, July 2001, 5 p.

[17] European Std. EN 50361, *Basic Standard for the Measurement of Specific Absorption Rate Related to Human Exposure to Electromagnetic Fields from Mobile Phones (300 MHz – 3 GHz)*, CENELEC, Brussels, Belgium, July 2001, 5 p.

[18] IEEE Std. 1528-2003, *IEEE Recommendation Practice for Determining the Peak Spatial-Average Specific Absorption Rate (SAR) in the Human Head from Wireless Communications Devices: Measurement Techniques*, IEEE, New York, USA, December 2003, 149 p.

[19] N. Kuster and Q. Balzano, "Energy absorption mechanism by biological bodies in the near field of dipole antennas above 300 MHz," *IEEE Transactions on Vehicular Technology*, vol. 41, no. 1, pp. 17-23, February 1992.

[20] O. Kivekäs, T. Lehtiniemi, and P.Vainikainen, "On the general energy-absorption mechanism in the human tissue," *Microwave and Optical Technology Letters*, vol. 43, no. 3, pp. 195-201, November 2004.

[21] H.- R. Chuang, "Numerical computation of fat layer effects on microwave near-field radiation to the abdomen of a full-scale human body model," *IEEE Transactions on Microwave Theory and Techniques*, vol. 45, no. 1, pp. 118-125, January 1997.

[22] R. E. Collin and S. Rothschild, "Evaluation of antenna *Q*," *IEEE Transactions on Antennas and Propagation*, vol. 12, no. 1, pp. 23-27, January 1964.

[23] R. L. Fante, "Quality factor of general ideal antennas," *IEEE Transactions on Antennas and Propagation*, vol. 17, no. 2, pp. 23-27, January 1969.

[24] R. C. Hansen, "Fundamental limitations in antennas," *Proceedings of the IEEE*, vol. 69, no. 2, pp. 170-182, February 1981.

[25] J. S. McLean, "Re-examination of the fundamental limits on the radiation *Q* of electrically small antennas," *IEEE Transactions on Antennas and Propagation*, vol. 44, no. 5, pp. 672-676, May 1996.

[26] W. Geyi, "Physical limitations of antenna," *IEEE Transactions on Antennas and Propagation*, vol. 51, no. 8, pp. 2116-2123, August 2003.

[27] R. King, C. W. Harisson, and D. H. Denton, "Transmission-line missile antennas," *IRE Transactions on Antennas and Propagation*, vol. 8, no. 1, pp. 88-90, January 1960.

[28] E. H. Newman, "Small antenna location synthesis using characteristic modes," *IEEE Transactions on Antennas and Propagation*, vol. 27, no. 4, pp. 530-531, July 1979.

[29] K. Sato, K. Matsumuto, K. Fujimoto, and K. Hirasawa, "Characteristics of a planar inverted-F antenna on a rectangular conducting body," *Electronics and Communications in Japan*, Part 1, vol. 72, no. 10, pp. 43-51, 1989.

[30] P. Vainikainen, J. Ollikainen, O. Kivekäs, and I. Kelander, *Effect of phone chassis on handset antenna performance*, Helsinki University of Technology, Radio Laboratory, Report S240, Espoo, Finland, 13 p, March 2000.

[31] P. Vainikainen, J. Ollikainen, O. Kivekäs, and I. Kelander, "Performance analysis of small antennas mounted on mobile handsets," *Proc. COST 259 Final Workshop – The Mobile Terminal and Human Body Interaction*, Bergen, Norway, April 2000, 8 p.

[32] D. Manteuffel, A. Bahr, and I. Wolff, "Investigation on integrated antennas for GSM mobile phones," *Proc. AP2000 Millennium Conference on Antennas and Propagation,* Davos, Switzerland, April 2000, CD-ROM SP-444 (ISBN 92-9092-776-3), paper p0587.pdf.

[33] A. T. Arkko and E. A. Lehtola, "Simulated impedance bandwidths, gains, radiation patterns and SAR values of a helical and a PIFA antenna on top of different chassis," *Proc. 11th International Conference on Antennas and Propagation (ICAP'01)*, UK, Manchester, April 2001, pp. 651-654.

[34] D. Manteuffel, A. Bahr, D. Heberling, and I. Wolf, "Design considerations for integrated mobile phone antennas," *Proc. 11th International Conference on Antennas and Propagation (ICAP'01)*, Boston, Massachusetts, April 2001, pp. 252-256.

[35] P. Vainikainen, J. Ollikainen, O. Kivekäs, and I. Kelander, "Resonator-based analysis of the combination of mobile handset antenna and chassis," *IEEE Transactions on Antennas and Propagation*, vol. 50, no. 10, pp. 1433-1444, October 2002.

[36] T.-Y, Wu and K.-L. Wong, "On the impedance bandwidth of a planar inverted-F antenna for mobile handsets," *Microwave and Optical Technology letters*, vol. 32, no. 4, pp. 249-251, February 2002.

[37] O. Kivekäs, J. Ollikainen, T. Lehtiniemi, and P. Vainikainen, "Bandwidth, SAR, and efficiency of internal mobile phone antennas," *IEEE Transactions on Electromagnetic Compatibility*, vol. 46, no. 1, pp. 71-86, February 2004.

[38] P. Pananyi, m. Al-Nuaimi, and P. Ivrissimtzis, "Near/far field and SAR of mobile communication antennas, *Proc. AP2000 Millennium Conference on Antennas and*

Propagation, Davos, Switzerland, April 2000, CD-ROM SP-444 (ISBN 92-9092-776-3), paper p0351.pdf.

[39] D. Manteuffel, A. Bahr, P. Waldow, and I. Wolff, "Numerical analysis of absorption mechanisms for mobile phones with integrated multiband antennas," *IEEE Antennas and Propagation Society International Symposium Digest*, vol. 3, Boston, USA, July 2001, pp. 82-85.

[40] R. Yamaguchi, K. Sawaya, Y. Fujinoto, and S. Adachi, "Effect of dimensions of conducting box on radiation pattern of monopole antenna for portable telephone," *IEICE Transaction on Communications*, vol. E76-B, no. 12, pp. 1526-1531, December 1993.

[41] J. Ollikainen, *Design an Implementation Techniques of Wideband Mobile Communications Antennas*, Ph.D. dissertation, Helsinki University of Technology, Radio Laboratory, Espoo, November 2004, 70 p.

[42] O. Kivekäs, *Design of High-Efficiency Antennas for Mobile Communications Devices*, Ph.D. dissertation, Helsinki University of Technology, Radio Laboratory, Espoo, August 2005, 50 p.

[43] L. Huang, W. L. Schroeder, and P. Russer, "Estimation of maximum attainable antenna bandwidth in electrically small mobile terminals," *Proc. 26th European Microwave Conference (EUMC'06)*, Manchester, UK, September 2006, pp. 630-633.

[44] R. J. Garbacz and R. H. Turpin, "A generalized expansion for radiated and scattered fields," *IEEE Transaction on Antennas and Propagation*, vol. 19, no. 3, pp. 348-358, May 1971.

[45] R. F. Harrington and J. R. Mautz, "Theory of characteristic modes for conducting bodies," *IEEE Transactions on Antennas and Propagation*, vol. 19, no. 5, pp. 622-628, September 1971.

[46] C. T. Famdie, W. L. Schroeder, and K. Solbach, "Numerical analysis of characteristic modes on the chassis of mobile phones," *European Conference on Antennas and Propagation (EUCAP'06)*, Nice, France, November 2006, CD-ROM, paper: 345145ct.pdf.

[47] M. Cabedo-Fabres, E. Antonino-Daviu, M. Ferrando-Bataller, and A. Valero-Nogueira, "On the use of characteristic modes to describe patch antenna performance," *Proc. IEEE Antennas and Propagation Society International Symposium Digest*, Columbus (Ohio), USA, June 2003, pp. 712-715.

[48] E. Antonino-Daviu, M. Cabedo-Fabres, M. Ferrando-Bataller, and J. Herranz-Herruzo, "Analysis of the coupled chassis-antenna modes in mobile handsets," *Proc. IEEE Antennas and Propagation Society International Symposium Digest*, Monterey (California), USA, June 2004, pp. 2751-2754.

[49] W. L. Schroeder, and C. T. Famdie, "Utilization and tuning of the chassis modes of a handheld terminal for the design of multiband radiation characteristics," *Proc. IEE*

Conference on Wideband and Multi-Band Antennas and Arrays, Birmingham, UK, September 2005, pp. 117-122.

[50] J. Rahola and J. Ollikainen, "Optimal antenna placement for mobile terminals using characteristic mode analysis," *Proc. European Conference on Antennas & Propagation (EUCAP'06)*, Nice, France, November, 2006, CD-ROM, file: 382996jr.pdf.

[51] Pat. FI114260, *Radiolaitteen modulaarinen kytkentärakenne ja kannettava radiolaite* (*Modular coupling structure for a radio device and a portable radio device*), P. Vainikainen, J. Ollikainen, O. Kivekäs, and I. Kelander, Finland, Appl. 20002529, 17.11.2000, (15.09.2004), 22 p.

[52] J. Villanen, *Compact antenna structure for mobile handsets*, M.S. thesis, Helsinki University of Technology, Radio Laboratory, Espoo, February 2003, 83 p.

[53] J. Villanen, J. Ollikainen, O. Kivekäs and P. Vainikainen, "Compact Antenna Structures for Mobile Handsets," *Proceedings of the COST 284*, Budabest, Hungary, April 2003.

[54] J. Villanen, J. Ollikainen, O. Kivekäs and P. Vainikainen, "Compact antenna structures for mobile handsets," *IEEE VTC2003 Fall Conference*, Orlando, Florida, October 2003, CD-ROM (0-7803-7955-1), paper 08A_02.pdf.

[55] J. Holopainen, J. Villanen, M. Kyrö, C. Icheln, and P. Vainikainen, "Antenna for handheld DVB-H terminal," *IEEE IWAT 2006 Small Antennas and Novel Metamaterials,* New York, USA, March 2006, CD-ROM (0-7803-9444-5), paper p077.pdf.

[56] W. L. Schroeder, A. A. Vila, and C. Thome, "Extremely small, wide-band mobile phone antennas by inductive chassis mode coupling," *Proc. 36th European Microwave Conference (EuMC'06)*, Manchester, UK, September 2006, pp. 1702-1705.

[57] M. Cabedo-Fabres, E. Antonino-Daviu, A. Valero-Nogueira, and M. Ferrando-Bataller, "Wideband radiating ground plane with notches," *Proc. IEEE Antennas and Propagation Society International Symposium Digest*, Washington, USA, July 2005, pp. 560-563.

[58] J. Holopainen, J. Villanen, C. Icheln, and P. Vainikainen, "Mobile terminal antennas implemented by using direct coupling," *Proc. European Conference on Antennas & Propagation (EUCAP'06)*, Nice, France, November, 2006, CD-ROM, file: 349858jh.pdf.

[59] D. Manteuffel, "Design of multiband antennas for the integration in mobile phones with optimized *SAR*," *IEEE Antennas and Propagation Society International Symposium Digest*, vol. 3, Columbus, Ohio, USA, June 2003, pp. 66-69.

[60] Z. D. Liu, P. S. Hall, and D. Wake, "Dual-frequency planar inverted-F antenna," *IEEE Transaction on Antennas and Propagation*, vol. 45, no. 10, pp. 1451-1458, October 1997.

[61] S. Tarvas and A. Isohätälä, “An internal dual-band mobile phone antenna,” *IEEE Antennas and Propagation Society International Symposium*, Salt Lake City, UT, USA, July 2000, vol. 1, pp. 266-269.

[62] M. Martínez-Vázquez and O. Litschke, "Quadband antenna for handeld personal communications devices", *IEEE Antennas and Propagation Society International Symposium*, vol. 1, Columbus-Ohio, USA, June 2003, pp. 455 - 458.

[63] G. Matthaei, L Young, and E. M. T. Jones, *Microwave Filters, Impedance-Matching Networks, and Coupling Structures*, 1964, Mc Graw-Hill, 1095 p.

[64] O. -S. Lin, C. -C. Liu, K. -M. Li, and C. H. Chen, “Design of an LTCC tri-band transceiver module for QPRS mobile applications,” *IEEE Transactions on Microwave Theory and Techniques*, vol. 52, no. 12, pp. 2718-2724, December 2004.

[65] L. K. Yeung, and K. -L. Wu, “A compact second-order LTCC bandpass filter with two finite transmission zeros,” *IEEE Transactions on Microwave Theory and Techniques*, vol. 51, no. 2, pp. 337-341, February 2003.

[66] A. Sutono, D. Heo, Y. -J. E. Chen, and J. Laskar, “High-Q LTCC-based passive library for wireless system-on-package (SOP) module development,” *IEEE Transactions on Microwave Theory and Techniques*, vol. 49, no. 10, pp. 1715-1724, October 2001.

[67] H. W. Bode, *Network Analysis and Feedback Amplifier Design*, New York, 1945, Van Nostrand, 551 p.

[68] R. M. Fano, “Theoretical limitations on the broadband matching of arbitrary impedances,” *Journal of the Franklin Institute*, vol. 249, no. 1, pp. 57-83, January 1950, and no. 2, pp. 139-154, February 1950.

[69] G. L. Matthaei, “Synthesis of Tchebycheff impedance-matching networks, filters, and interstages,” *IRE Transactions on Circuit Theory*, vol. CT-3, no. 3, pp. 163-172, September 1956.

[70] W.- K. Chen and T. Chaisrakeo, “Explicit formulas for the synthesis of optimum bandpass Butterworth and Chebyshev impedance-matching networks,” *IEEE Transactions on Circuits and Systems*, vol. 27, no. 10, pp. 928-942, October 1980.

[71] B. S. Yarman and H. J. Carlin, “A simplified “real frequency” technique applied to broad-band multistage microwave amplifiers,” *IEEE Transactions on Microwave Theory and Techniques*, vol. 30, no. 12, pp. 2216-2222, December 1982.

[72] H. An, B. K. J. C. Nauwelaers, and A. R. Van de Capelle, “Broadband microstrip antenna design with the simplified real frequency technique,” *IEEE Transaction on Antennas and Propagation*, vol. 42, no. 2, pp. 129-136, February 1994.

[73] P. Lindberg, M. Sengul, E. G. Cimen, B. S. Yarman, A. Rydberg, and A. Aksen, “A single matching network design for a dual band PIFA antenna via simplified real

frequency technique," *Proc. European Conference on Antennas & Propagation (EUCAP'06)*, Nice, France, November, 2006, CD-ROM, file: 363826pl.pdf.

[74] F. J. Witt, "Optimum lossy matching networks for resonant antennas," *Proc. IEEE Antennas and Propagation Society International Symposium Digest*, vol. 3, San Jose, CA, USA, June 1989, pp. 1360-1363.

[75] F. J. Witt, "Optimum lossy broadband matching networks for resonant antennas," *RF Design*, vol. 13, no. 4, pp. 44-51, April 1990, and no. 7, p. 10, July 1990.

[76] J. Anguera, C. Puente, J. Romeu, C. Borja, and G. Font, "An optimum method to design probe-fed single-layer single-patch wideband microstrip antenna," *Proc. AP2000 Millennium Conference on Antennas and Propagation*, Davos, Switzerland, April 2000, CD-ROM SP-444 (ISBN 92-9092-776-3), paper p1023.pdf.

[77] J. Ollikainen and P. Vainikainen, *Design and bandwidth optimization of dual-resonant patch antennas*, Helsinki University of Technology, Radio Laboratory, Report S 252, Espoo, Finland, 41 p, March 2002.

[78] M. Sager, M. Forcucci, and T. Kristensen, "A novel technique to increase the realized efficiency of a mobile phone antenna placed beside a head-phantom," *IEEE Antennas and Propagation Society International Symposium Digest*, vol. 2, Columbus, Ohio, USA, June 2003, pp. 1013-1016.

[79] J. Villanen, J. Holopainen, O. Kivekäs, and P. Vainikainen, "Mobile broadband antennas," *URSIGA 2005 conference,* New Delhi, India, October 2005, file BC.2(01464).pdf.

[80] US patent application, *Quad-band coupling element antenna structure*, Nokia Corporation, Espoo, Finland, (S. Ozden, B. Nielsen, C. Jorgensen, J. Villanen, C. Icheln, and P. Vainikainen), Appl. 11/321,016, 28.12.2005, 34 p.

[81] K.- L. Wong, G.- Y. Lee, and T.- W. Chiou, "A low-profile planar monopole antenna for multiband operation of mobile handsets," *IEEE Transaction on Antennas and Propagation*, vol. 51, no. 1, pp. 121-124, February 2003.

[82] X. Jing, Z. Du, and K. Gong, "Compact planar monopole antenna for multi-band mobile phones," *Proc. Asia-Pacific Microwave Conference (APMC'05)*, vol. 4, Suzhou, China, December 2005, 4 p.

[83] A. Thornell-Pers and P. Erlandsson, "Compact active multiband cellular antenna for mobile handsets," *Proc. International Workshop on Antenna Technologies Conference (IWAT'07)*, Cambridge, UK, March 2007, pp. 81-84.

[84] J. Ollikainen and P. Vainikainen, "Radiation and bandwidth characteristics of two planar multistrip antennas for mobile communication systems," *Proc. 48th IEEE Vehicular Technology Conference (VTC'98)*, vol. 2, Ottawa, Ontario, Canada, May 1998, pp. 1186-1190.

[85] P. Ciais, R. Staraj, G. Kossiavas, and C. Luxey, "Design of an internal quad-band antenna for mobile phones," *IEEE Microwave and Wireless Components Letters*, vol. 14, no. 4, pp. 148-150, April 2004.

[86] S.- H. Yeh, K.- L. Wong, T.- W. Chiou, and S.- T. Fang, "Dual-band planar inverted F antenna for GSM/DCS mobile phones," *IEEE Transaction on Antennas and Propagation*, vol. 51, no. 5, pp. 1124-1126, May 2003.

[87] G.- Y. Lee and K.- L. Wong, "Quad-band internal monopole mobile phone antenna," *Microwave and Optical Technology Letters*, vol. 40, no. 5, pp. 359-361, March 2004.

[88] Y. Li, T. Cantin, B. Derat, D. Pasquet, and J.- C. Bolomey, "Application of resonant matching circuits for simultaneously enhancing the bandwidths of multi-band mobile phones," *Proc. International Workshop on Antenna Technologies Conference (IWAT'07)*, Cambridge, UK, March 2007, pp. 479-482.

[89] J. Ollikainen, O. Kivekäs, C. Icheln, and P. Vainikainen, "Internal multiband handset antenna realized with an integrated matching circuit," *Proc. 12th International Conference on Antennas and Propagation (ICAP'03)*, Exeter, UK, March-April 2003, pp. 629-632.

[90] O. Kivekäs, J. Ollikainen, and P. Vainikainen, "Frequency-tunable internal antenna for mobile phones," *Proc. 12th International Symposium on Antennas (JINA'02)*, vol. 2, Nice, France, November 2002, pp. 53-56.

[91] Pat. US6674411 B2, *Antenna arrangement*, Koninklijke Philips Electronics N.V., The Netherlands, (K. Boyle), Appl. 10/085696, 27.02.2002, (06.01.2004), 6 p.

[92] W. L. Schroeder, P. Schmitz, and C. Thome, "Miniaturization of mobile phone antennas by utilization of chassis mode resonances", *Proc. German Microwave Conference (GeMIC'06)*, no. 7b-3, Karlsruhe, Germany, March 2006.

[93] J. Holopainen, *Antenna for handheld DVB terminal*, M.S. thesis, Helsinki University of Technology, Radio Laboratory, Espoo, May 2005, 93 p.

[94] P. Lindberg and E. Öjefors, "A bandwidth enhancement technique for mobile handset antennas using wavetraps," *IEEE Transaction on Antennas and Propagation*, vol. 54, no. 8, pp. 2226-2233, August 2006.

[95] J. Holopainen, J. Villanen, M. Kyrö, C. Icheln, and P. Vainikainen, "Terminal Antenna for DVB-H Reception," *Presented in the COST 284 meeting*, Dubrovnik, Croatia, October 2005.

[96] EICTA, *Mobile and portable DVB-T radio access interface specification*, version 1.0, 8.3.2004.

[97] J. Ollikainen, O. Kivekäs, and P. Vainikainen, "low-loss tuning circuits for frequency-tunable small resonant antennas," *Proc. 13th IEEE International Symposium on Personal, Indoor and Mobile Radio Communications (PIMRC'02)*, Lisboa, Portugal, September 2002, pp. 1882-1887.

[98] P. Lindberg, E. Öjefors, and A. Rydberg, "Wideband slot antenna for low-profile hand-held terminal applications," *Proc. 26th European Microwave Conference (EUMC'06)*, Manchester, UK, September 2006, pp. 1698-1701.

[99] P.- L. Teng, T.- W. Chiou, and K.- L. Wong, "Planar inverted-F antenna with a bent meandered radiating arm for GSM/DCS operation," *Microwave and Optical Technology Letters*, vol. 38, no. 1, pp. 73-75, July 2003.

[100] P.- L. Teng, C.- Y. Chiu, and K.- L. Wong, "Internal planar monopole antenna for GSM/DCS/PCS folder-type mobile phones," *Microwave and Optical Technology Letters*, vol. 39, no. 2, pp. 106-108, October 2003.

[101] C.-Y. Chiu, and K.-L. Wong, "An internal metal-plate antenna for a folder-type mobile phone," *Microwave and Optical Technology Letters*, vol. 42, no. 4, pp. 294-296, August 2004.

[102] K.-L. Wong, S.-W. Su, C.-L. Tang, and S.-H. Yeh, "Internal shorted patch antenna for a UMTS folder-type mobile phone," *IEEE Transactions on Antennas and Propagation*, vol. 53, no. 10, pp. 3391 – 3394, October 2005.

[103] S. Gabriel, R. W. Lau, and C. Gabriel, "The dielectric properties of human body tissues: III. Parametric models for the dielectric spectrum of tissues," *Physics in Medicine and Biology*, vol. 41, no. 11, pp. 2271-2293, November 1996.

[104] M. Mikkola, *Effect of Complex Handset Structures on Antenna Performance*, M. S. thesis, Helsinki University of Technology, Radio Laboratory, Finland, October, 2005, 102 p.

[105] W. C. Jakes, Y. S. Yeh, M. J. Gans, and D. O. Reudink, "Fundamentals of diversity systems," Chapter 5 in *Microwave Mobile Communications*, Editor W. C. Jakes, New York, John Wiley & Sons, 1974, 642 p.

[106] R. G. Vaughan and J. Bach Andersen, "Antenna diversity in mobile communications," *IEEE Transactions on Vehicular Technology*, vol. 36, no. 4, pp. 149-172, November 1987.

[107] C. B. Dietrich, K. Dietze, J. R. Nealy, and W. L. Stutzman, "Spatial, polarization, and pattern diversity for wireless handheld terminals," *IEEE Transactions on Antennas and Propagation*, vol. 49, no. 9, pp. 1271 - 1281, September 2001.

[108] G. J. Foschini, "Layered space-time architecture for wireless communication in a fading environment when using multielement antennas," *Bell Labs technical Journal*, pp. 41-59, Autumn 1996.

[109] G. J. Foschini, G. D. Golden, R. A. Valenzuela, and P. W. Wolniansky, "Simplified processing for wireless communication at high spectral efficiency," *IEEE Journal on Selected Areas in Communications – Wireless Communications Series*, vol. 17, pp. 1841 – 1852, November 1999.

[110] I. E. Telatar, “Capacity of multi-antenna Gaussian channels,” *AT&T Bell Labs Technical memorandum*, 28 p, October 1995.

[111] G. J. Foschini, M. J. Gans, “On the limits of wireless communications in a fading environment when using multiple antennas,” *Wireless Personal Communications*, vol. 6, no. 3, pp. 311–335, March 1998.

[112] V. Tarokh, N. Seshadri, and A. R. Calderbank, “Space-time codes for high data rate wireless communication: Performance criterion and code construction,” *IEEE Transactions on Information Theory*, vol. 44, no. 2, pp. 744-765, March 1998.

[113] S. Alamouti, “A simple transmit diversity technique for wireless communications,” *IEEE Journal on Selected Areas in Communications*, vol. 16, no. 8, pp. 1451-1458, October 1998.

[114] K. Kalliola, K. Sulonen, H. Laitinen, O. Kivekäs, J. Krogerus, and P. Vainikainen, “Angular power distribution and mean effective gain of mobile antenna in different propagation environments,” *IEEE Transactions on Vehicular Technology*, vol. 51, no. 5, pp. 823 -838, September 2002.

[115] K. Sulonen and P. Vainikainen, “Performance of mobile phone antennas including effect of environment using two methods,” *IEEE Transactions on Instrumentation and Measurement*, vol. 52, no. 6, pp. 1859-1864, December 2003.

[116] T. Taga, “Analysis for mean effective gain of mobile antennas in land mobile radio environments,” *IEEE Transactions on Vehicular Technology*, vol. 39, no. 2, pp. 117-131, May 1990.

[117] A. M. D. Turkmani, A. A. Arowojolu, P. A. Jefford, and C. J. Kellett, “An experimental evaluation of the performance of two-branch space and polarization diversity schemes at 1800 MHz,” *IEEE Transactions on Vehicular Technology*, vol. 44, no. 2, pp. 318-326, May 1995.

[118] P. Suvikunnas, J. Salo, J. Kivinen, and P. Vainikainen, “Empirical comparison of MIMO antenna configurations,” *IEEE Vehicular Technology Conference (VTC’2005 Spring)*, Stockholm, Sweden, June 2005, vol. 1, pp. 53 – 57.

[119] C. Waldschmidt, S. Schulteis, and W. Wiesbeck, “Complete RF system model for analysis of compact MIMO arrays,” *IEEE Transactions on Vehicular Technology*, vol. 53, no. 3, pp. 579 – 586, May 2004.

[120] C.- N. Chuah, D. N. C. Tse, J. M. Kahn, and R. A. Valenzuela, “Capacity scaling in MIMO wireless systems under correlated fading,” *IEEE Transactions on Information Theory*, vol. 48, no. 3, pp. 637-650, March 2002.

[121] Ö. Oyman, R. U. Nabar, H. Bölcskei, and A. J. Paulraj, “Characterizing the statistical properties of mutual information in MIMO channels,” *IEEE Transactions on Signal Processing*, vol. 51, no. 11, pp. 2784-2795, November 2003.

[122] N. Chiurtu, B. Rimoldi, and E. Telatar, "On the capacity of multi-antenna gaussian channels," *Proc. IEEE International Symposium on Information Theory (ISIT'01)*, Washington, USA, June 2001, p. 53.

[123] D.– S. Shiu, G. J. Foschini, M. J. Gans, and J. M. Kahn, "Fading correlation and its effect on the capacity of multielement antenna systems," *IEEE Transactions on Communications*, vol. 48, no. 3, pp. 502 – 513, March 2000.

[124] J. Salo, P. Suvikunnas, H. M. El-Sallabi, and P. Vainikainen, "Some insights into MIMO mutual information: the high SNR case," *IEEE Transactions on Wireless Communications*, vol. 5, no. 11, pp. 2997 - 3001, November 2006.

[125] P. Suvikunnas, K. Sulonen, J. Villanen, C. Icheln and P. Vainikainen, "Evaluation of performance of multi-antenna terminals using two approaches," *Proc. IEEE Instrumentation and Measurement Technology Conference (IMTC'04)*, Como, Italy, May 2004, pp. 1091-1096.

[126] J. Kivinen, T. Korhonen, P. Aikio, R. Gruber, P. Vainikainen and S.-G. Häggman, "Wideband radio channel measurement system at 2 GHz," *IEEE Transactions on Instrumentation and Measurement*, vol. 48, pp. 39–44, February 1999.

[127] K. Kalliola, H. Laitinen, L. Vaskelainen, and P. Vainikainen, "Real-time 3-D spatial-temporal dual-polarized measurement of wideband radio channel at mobile channel," *IEEE Transactions on Instrumentation and Measurement*, vol. 49, no. 2, pp. 439-448, April 2000.

[128] B. H. Fleury, M. Tschudin, R. Heddergott, D. Dahlhaus, and K. I. Pedersen, "Channel parameter estimation in mobile radio environments using the SAGE algorithm," *IEEE Journal on Selected Areas of Communication*, vol. 17, no. 3, pp. 434-450, March 1999.

[129] G. F. Pedersen, S. Widell, and T. Ostervall, "Handheld antenna diversity evaluation in a DCS 1800 small cell," *The 8th IEEE International Symposium on Personal, Indoor and Mobile Radio Communications (PIMRC)*, vol. 2, September 1997, pp. 584 – 588.

[130] B. M. Green, and M. A. Jensen, "Diversity performance of dual-antenna handsets near operator tissue," *IEEE Transactions on Antennas and Propagation*, vol. 48, no. 7, pp. 1017 - 1024, July 2000.

[131] C. C. Chiau, X. Chen, and C. G. Parini, "A compact four-element diversity-antenna array for PDA terminals in a MIMO system," *Microwave and Optical Technology Letters*, vol. 44, no. 5, pp. 408 – 412, March 2005.

[132] M. Karaboikis, C. Soras, G. Tsachtsiris, and V. Makios, "Compact dual-printed inverted-F antenna diversity systems for portable wireless devices," *IEEE Antennas and Wireless Propagation Letters*, vol. 3, no. 1, pp. 9 – 14, 2004.

[133] Z. Ying, T. Bolin, V. Plicanic, A. Derneryd, and G. Kristensson, "Diversity antenna terminal evaluation," *Proc. IEEE Antennas and Propagation Society International Symposium*, Washington, USA, vol. 2A, July 2005, pp. 375 – 378.

[134] Y. Zhinong, V. Plicanic, T. Bolin, G. Kristensson, and A. Derneryd, "Characterization of multi-channel antenna performance for mobile terminal by using near field and far field parameters," *Proc. of the COST 273 TD(04)(095) meeting*, Göteborg, Sweden, June 2004.

[135] W. A. T. Kotterman, G. F. Pedersen, and K. Olesen, "Diversity properties of multiantenna small handheld terminals," *EURASIP Journal on Applied Signal Processing (Special Issue on Smart Antennas)*, vol. 9, pp.1340 - 1353, August 2004.

[136] A. Diallo, C. Luxey, P. L. Thuc, R. Staraj, and G. Kossiavas, "Study and reduction of the mutual coupling between two mobile phone PIFAs operating in the DCS1800 and UMTS bands," *IEEE Transactions on Antennas and Propagation*, vol. 54, no. 11, pp. 3063 – 3074, November 2006.

[137] J. Thaysen and K. B. Jakobsen, "MIMO channel capacity versus mutual coupling in multi antenna element systems," *26th Antenna Measurement Techniques Association Meeting and Symposium (AMTA'04)*, Atlanta, GA, October 2004.

[138] B. Lindmark, L. Garcia-Garcia, N. Jalden, and C. Orlenius, "Evaluation of MIMO arrays using antenna patterns, reverberation chamber, and channel measurements," *European Conference on Antennas and Propagation (EuCAP'06)*, Nice, France, November 2006, CD-ROM, paper 372151bl.pdf.

[139] D. W. Browne, M. Manteghi, M. P. Fitz, and Y. Rahmat-Samii, "Experiments with compact antenna arrays for MIMO radio communications," *IEEE Transactions on Antennas and Propagation*, vol. 54, no. 11, pp. 3239 – 3250, November 2006.

[140] C. Waldschmidt, C. Kuhnert, S. Schulteis, and W. Wiesbeck, "On the integration of MIMO systems into handheld devices," *Proc. ITG Workshop on Smart Antennas*, München, Germany, March 2004, pp. 1 - 8.

[141] J. Salo, B. Badic, P. Suvikunnas, H. Weinrichter, M. Rupp, and P. Vainikainen, "Performance of space-time block codes in urban microcells: the effect of antennas," *International Symposium on Wireless Personal Multimedia Communications (WPMC'05)*, Aalborg, Denmark, September 2005, pp. 1848 - 1852.

[142] K. Boyle, "Radiation patterns and correlation of closely spaced linear antennas," *IEEE Transactions on Antennas and Propagation*, vol. 50, no. 8, pp. 1162-1165, August 2002.